226
C.2
UCRL-53558

UCRL-53558

SAI
T&MSS
LIBRARY

Petrologic and Geochemical Characterization of the Topopah Spring Member of the Paintbrush Tuff: Outcrop Samples Used in Waste Package Experiments

K. G. Knauss

June 1984

Lawrence Livermore National Laboratory

DISCLAIMER

This document was prepared as an account of work sponsored by an agency of the United States Government. Neither the United States Government nor the University of California nor any of their employees, makes any warranty, express or implied, or assumes any legal liability or responsibility for the accuracy, completeness, or usefulness of any information, apparatus, product, or process disclosed, or represents that its use would not infringe privately owned rights. Reference herein to any specific commercial products, process, or service by trade name, trademark, manufacturer, or otherwise, does not necessarily constitute or imply its endorsement, recommendation, or favoring by the United States Government or the University of California. The views and opinions of authors expressed herein do not necessarily state or reflect those of the United States Government or the University of California, and shall not be used for advertising or product endorsement purposes.

Work performed under the auspices of the U.S. Department of Energy by Lawrence Livermore National Laboratory under Contract W-7405-Eng-48.

UCRL-53558
Distribution Category UC-70

Petrologic and Geochemical Characterization of the Topopah Spring Member of the Paintbrush Tuff: Outcrop Samples Used in Waste Package Experiments

K. G. Knauss

Manuscript date: June 1984

SAI
T&MSS
LIBRARY

T&MSS
LIBRARY

LAWRENCE LIVERMORE NATIONAL LABORATORY
University of California • Livermore, California • 94550

Available from: National Technical Information Service • U.S. Department of Commerce
5285 Port Royal Road • Springfield, VA 22161 • $8.50 per copy • (Microfiche $4.50)

Contents

Abstract 1
Introduction 1
Sample Locality 2
Preparation of Crushed Tuff 8
Petrographic Description 8
Bulk Mineralogy via XRD 18
Bulk Chemistry via NAA 20
Surface Area of Crushed Tuff 21
Individual Mineral Phase Chemistry via EMP 21
Summary 34
Acknowledgments 35
References 36

Petrologic and Geochemical Characterization of the Topopah Spring Member of the Paintbrush Tuff: Outcrop Samples Used in Waste Package Experiments

Abstract

This report summarizes characterization studies conducted with outcrop samples of Topopah Spring Member of the Paintbrush Tuff (Tpt). In support of the Waste Package Task within the Nevada Nuclear Waste Storage Investigation (NNWSI), Tpt is being studied both as a primary object and as a constituent used to condition water that will be reacted with waste form, canister, or packing material. These studies directly or indirectly support NNWSI subtasks concerned with waste package design and geochemical modeling. To interpret the results of subtask experiments, it is necessary to know the exact nature of the starting material in terms of the initial bulk composition, mineralogy, and individual phase geochemistry.

Introduction

A location at Yucca Mountain adjacent to the Nevada Test Site has been studied as a potential location for a mined geologic repository for high-level nuclear waste. Four tuff units in the Southern Nevada volcanic field were identified as candidate horizons for the repository. Two units (Tram Member and Bullfrog Member of the Crater Flat Tuff) are situated below the static water level within the block at Yucca Mountain, while the other two units (Bedded Tuff of Calico Hills and the Topopah Spring Member of the Paintbrush Tuff) are in the unsaturated zone (Bish et al., 1981). Early Waste Package experiments focused on the saturated zone, specifically the Bullfrog Member tuff (Oversby and Knauss, 1983; Knauss, 1983). However, in late 1982 the focus shifted to the unsaturated zone and the Topopah Spring Member of the Paintbrush Tuff (Tpt). All subsequent Waste Package experiments used Tpt as the potential repository horizon. When the decision was made to concentrate on the unsaturated zone, it became necessary to define the potential repository horizon within the unit. On the basis of correlation of core logs, geophysical logs, mineralogy, and physical properties from holes USW G-1, USW G-2, UE-25a#1, and UE-25b#1, the repository horizon was defined as an interval 997 to 1285 ft referenced to hole USW G-1 (Tyler, 1982).

Although drillcore samples are available from a number of locations within and around the repository block, only relatively small quantities of core are available for destructive testing. Because much of the materials testing being done at Lawrence Livermore National Laboratory (LLNL) requires not only large amounts of tuff to condition water but also material cylinders larger in diameter (up to 6 in.) than the core typically available, it was necessary to use outcrop samples for many of the Waste Package experiments. Outcrop samples were obtained from a position in the column stratigraphically equivalent to the proposed repository interval; the location selected allowed easy access for sampling the large quantities needed. For the detailed rock/water interaction studies to be modeled by the geochemical modeling code EQ3/6, which will be used to establish the package environment, drill-hole samples from appropriate depth in USW G-1 are being used, in addition to samples from other drill cores and outcrop samples.

The mineralogic and geochemical character of the tuff must be characterized for two reasons:

- To understand the hydrothermal interaction between the tuff and water in the waste package environment, and
- To serve as a baseline against which to compare the results of more complex component interaction testing in which rock, water, and other materials are involved.

The analytical techniques used to characterize this outcrop Tpt include: transmitted- and reflected-light optical microscopy, x-ray diffraction analyses (XRD), neutron activation analyses (NAA), gas adsorption surface area analyses (BET), scanning electron microscopy (SEM), and electron microprobe analyses (EMP) with both semiquantitative energy-dispersive spectrometry (EDS) and quantitative wavelength-dispersive spectrometry (WDS).

This report summarizes the characterization of Tpt outcrop material that will be used by experimenters conducting subtasks within the Waste Package Task at LLNL, as well as by outside contractors conducting experiments on our behalf. It provides data on the mineralogy and geochemistry of the outcrop Tpt samples and also establishes this outcrop material as a suitable equivalent to the material present at depth beneath Yucca Mountain within the proposed repository interval.

Sample Locality

Because it was necessary to collect material from outcrop that represents rock at depth beneath Yucca Mountain, the nature of ash flow tuffs and the nature of the proposed repository horizon are described below. This discussion will illustrate the criteria used to select the appropriate outcrop and provide some of the information used to assign its relative stratigraphic position within the column.

As originally described by Lipman et al. (1966), Tpt is a multiple-flow compound cooling unit. Welding and crystallization zones within the unit are well developed and typical for a thick ignimbrite: a large core of densely welded devitrified material overlain by nonwelded tuff and underlain by a welded but glassy vitrophyre and nonwelded tuff. Deviations from simple cooling are slight; however, individual flow units within the densely welded core are recognizable by concentration of pumice blocks and lithic inclusions and by the presence of thin zones of lithophysal cavities, vapor-phase alteration, or both. As observed in outcrop where the unit is thicker than 250 ft, a main lithophysal zone is developed within the densely welded devitrified core. Compositionally the Tpt may be also described as zoned in that a quartz latite, phenocryst-rich, cap rock overlies a phenocryst-poor, high-silica rhyolite that forms the major part of the unit.

If the 700-ft-thick Busted Butte type section is used as an example, typical zonation can be described in this way: In the first 85–100 ft (progressing from the bottom) of the Tpt one moves from a basal nonwelded, glassy zone (Fig. 1) into a zone of partial welding (Fig. 2), and then into the densely welded, glassy vitrophyre (Fig. 3). Overlying the vitrophyre is 240 ft of densely welded, devitrified, crystal-poor tuff, which is generally light gray to grayish-red to pale reddish-brown (mottled) and in places slightly vapor-phase-altered (Fig. 4). In the upper 50 ft of this interval lithophysal cavities begin to appear, but they are small, scattered, flattened, and frequently filled

Figure 1. Busted Butte type section. Nonwelded, glassy base of Tpt containing large pumice blocks overlying an older bedded tuff.

Figure 2. Busted Butte type section. Partly welded zone containing blackened pumice just below the vitrophyre.

Figure 4. Busted Butte type section. Crystal-poor, densely welded, devitrified, high-silica rhyolite between the main lithophysal zone and the vitrophyre.

Figure 3. Busted Butte type section. Densely welded, black vitrophyre.

with the products of vapor-phase alteration, i.e., quartz and alkali feldspar (Fig. 5). This interval is overlain by another 245 ft of densely welded, devitrified, but highly lithophysal tuff—the main lithophysal zone (Fig. 6), where the cavities are now large, closely spaced, and nearly circular in cross section. For the next 50 ft the tuff is again densely welded and nonlithophysal, but vapor-phase-altered. Within another 20 ft the tuff grades into a more crystal-rich, quartz latite cap rock. The densely welded, devitrified cap rock continues for 40 ft and is overlain by a 25-ft-thick glassy section that ranges from a densely welded upper vitrophyre to partly welded, and finally nonwelded, tuff.

This general description from Lipman et al. (1966) of the Tpt section also fits reasonably well the main features of Tpt as it is encountered in drillholes beneath Yucca Mountain, with two notable exceptions:

- The Tpt section beneath Yucca Mountain (Fig. 7) to the west of Busted Butte is from 1000 to 1200 ft thick.
- The densely welded, devitrified core of the rhyolitic interval contains two lithophysal

Figure 5. Busted Butte type section. Top of interval shown in Fig. 4 where small, scattered, flattened lithophysal appear and are frequently filled with the products of vapor-phase alteration.

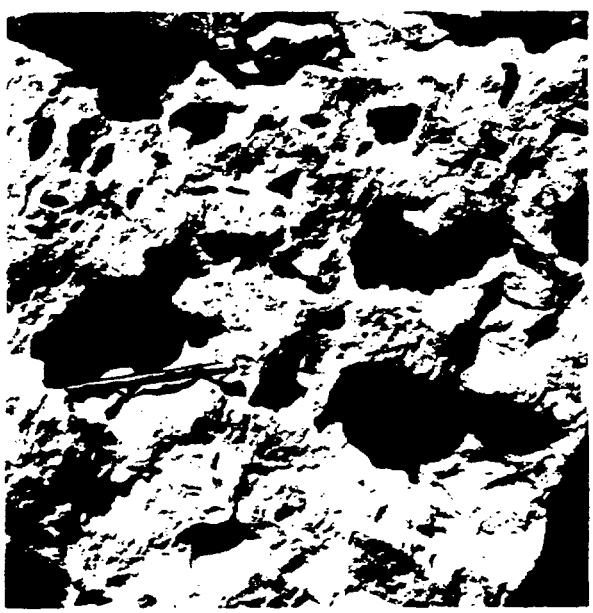

Figure 6. Busted Butte type section. Main lithophysal zone, densely welded, devitrified, but highly lithophysal with large, closely spaced, nearly circular cavities.

zones separated by additional densely welded, devitrified, vapor-phase-altered rhyolite (Spengler et al., 1981; Scott and Castellanos, 1983).

These differences suggest that at the time of Tpt deposition the area to the east of Yucca Mountain (Busted Butte) was already topographically high. Thus thicker intervals of the same flow units, or additional but less voluminous flow units, or a combination of the two, may be present at Yucca Mountain, but never reached Busted Butte.

The proposed repository interval within the Tpt, as previously defined by depth equivalence to USW G-1 (Tyler, 1982), corresponds to the interval in the rhyolitic tuff from the base of the lower lithophysal zone to the top of the lower vitrophyre. This interval is densely welded, devitrified, vapor-phase-altered, crystal-poor rhyolite. As suggested by Crowe (1984), an easily accessible interval of Tpt with these general characteristics is exposed in outcrop at NTS coordinates 745,500'N and 573,500'E (location Tpt-FR on Fig. 7) on the extreme southwest end of Fran Ridge. This location is about 3000 ft south of the pad for UE-25h#1, the horizontal drillhole in Fran Ridge (Fig. 8). Tpt-FR is the sample locality for all outcrop material used in the Waste Package experimental program.

At this location the Tpt fits the general description for the proposed repository horizon; however, it does contain relatively large and extremely flattened lithophysal cavities (Fig. 9) and is highly fractured. Because the Tpt dips to the east at Fran Ridge, we should be somewhat lower in the section than the pad at UE-25h#1; however, several faults between the two locations actually put us slightly higher. A view from the east looking at UE-25h#1 and the south end of Fran Ridge (Fig. 10) shows a ledge on the skyline formed by a vapor-phase-altered (harder) major lithophysal zone above the pad. This resistant lithophysal zone may be followed to the south toward Tpt-FR across the two previously mapped (Lipman and McKay, 1965) northeast-trending normal faults (which re-expose it) and an unmapped northwest-trending fault just above the Tpt-FR site (Fig. 8). Although the Tpt at the UE-25h#1 pad looks almost identical to that at Tpt-FR, it is nonlithophysal. However, less than 30 ft above the pad large, flattened lithophysal cavities begin to appear at the base of a major lithophysal zone. This field evidence and the macroscopic characteristics observable in hand specimen fix the relative position of Tpt-FR at the base of the lithophysal zone at Fran Ridge and only slightly higher in the section than UE-25h#1, which was intended to penetrate rock similar to that expected at the repository level. Structural complications

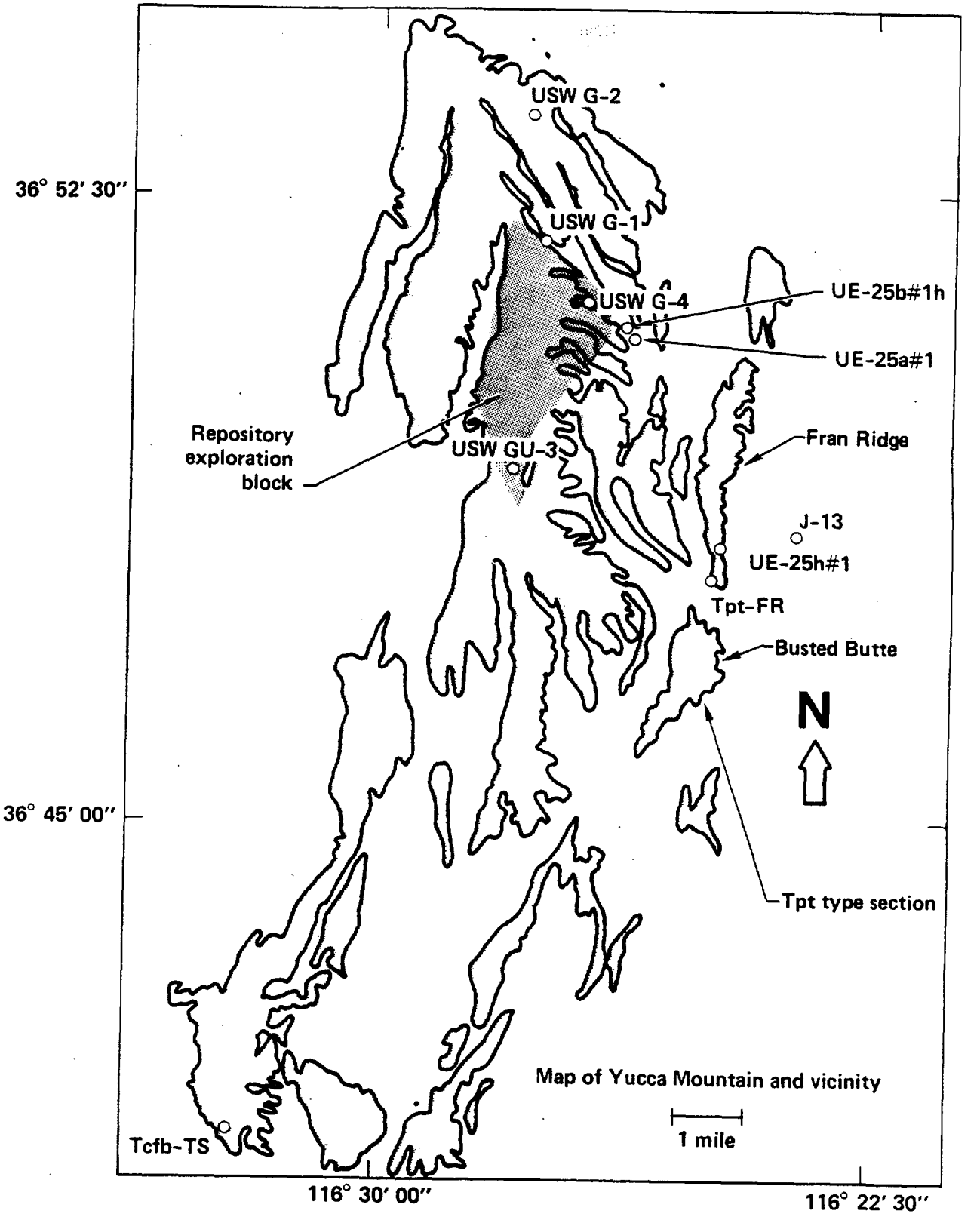

Figure 7. Map of Yucca Mountain and vicinity.

Figure 8. View of south end of Fran Ridge from Busted Butte.

Figure 9. Tpt-FR locality. Highly fractured, densely welded, devitrified, vapor-phase-altered, crystal-poor rhyolite containing large, flattened lithophysae.

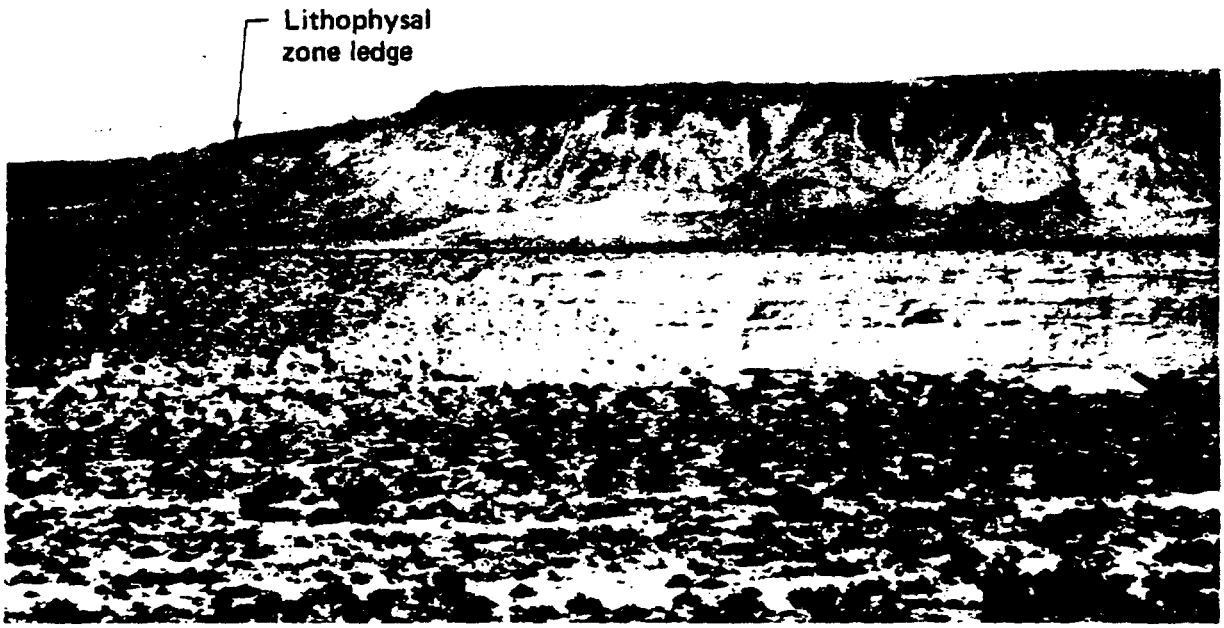

Figure 10. View of the southeast end of Fran Ridge from J-13 showing UE-25h#1 and ledge of resistant material near the base of the main lithophysal zone.

may preclude correlating the stratigraphic position of Tpt-FR with the type section at Busted Butte (Crowe, 1984). However, in hand specimen the Tpt-FR material closely resembles that collected at Busted Butte locations, which would place Tpt-FR near the very base (certainly within 50 ft) of the main lithophysal zone.

The discussion above has served to locate Tpt-FR relative to the Tpt section exposed at Fran Ridge above UE-25h#1 and at the Busted Butte type section; however, it cannot unambiguously locate Tpt-FR relative to the proposed repository horizon beneath Yucca Mountain. The field evidence and macroscopic observations in hand sample allow us to confidently place Tpt-FR between the base of the upper lithophysal zone and the lower vitrophyre, but we cannot say we are between the base of the lower lithophysal zone and the vitrophyre. Evidence to be presented in following sections on petrography, bulk mineralogy, and phenocryst chemistry will help to resolve this question. Furthermore, evidence that will be given in subsequent reports on hydrothermal rock/water interaction studies will show that—for conditioning water—material from the densely welded, devitrified, vapor-phase-altered Tpt from either above or below the lowermost lithophysal zone may be used.

It should be noted that at Tpt-FR an arroyo draining Yucca Mountain passes within a few tens of feet of the outcrop, and abundant caliche fills fractures in the tuff (Fig. 9). The Tpt exposed at UE-25h#1 contains even more abundant caliche. The rock is expected to contain a readily soluble fraction of material filling pores and fractures in the rock, and this effect is seen in rock/water experiments performed with tuff that has not been specifically pretreated to remove this material (Knauss et al., 1983).

Preparation of Crushed Tuff

At the Tpt-FR sample locality large blocks of the densely welded tuff were easily removed because the rock is highly fractured. An effort was made to avoid blocks containing more than a few of the flattened lithophysal cavities. The blocks were boxed, labeled, and shipped to LLNL for further sample preparation. All material that was removed came from an interval spanning less than 10 ft in the Tpt section. Over this interval in hand sample the Tpt appeared to be completely uniform.

Upon arrival at LLNL the next step was to trim the blocks with a large rock saw to remove the effects of weathering along joints in the tuff. At this point the large, cleaned-up, and squared-off blocks were used to make cores ranging from 1 to 6 in. in diameter for various parts of the experimental program. This included the glass-waste-form testing being done in tuff reaction vessels (at Savannah River National Laboratory), the permeability measurements being made in a thermal gradient (at USGS), the permeability measurements being made in an isothermal apparatus (at LLNL), and the hydrothermal rock/water interaction experiments being done with polished core wafers (at LLNL). Several polished core wafers prepared at this point were also used in the EMP characterization detailed below. For crushed tuff, the blocks were slabbed on a smaller rock saw into slabs less than 1 in. thick; the slabs were then processed in a large jaw crusher. At this point several slabs were removed from further processing for the start of the sample characterization process. Polished thin sections and crushed tuff were prepared for whole rock XRD, petrography, EMP, and NAA analyses as a part of the characterization. Part of the slabbed material was also supplied with no further pretreatment to Westinghouse Hanford Company for Zircaloy-cladding corrosion experiments.

Two sizes of material were prepared for the parts of the Waste Package Task requiring crushed tuff:

- Slabbed material was passed through a jaw crusher set to produce material with an average diameter of 1 mm. This material was supplied as is to the metallurgists for corrosion experiments in support of canister development.
- An additional crushing step was required to provide outcrop material for experimenters conducting accelerated testing to provide baseline values (rock/water only) for the Package Environment subtask in the Waste Package Task. The mm-size particles were further crushed in a flat plate grinder with high-purity alumina plate and then sieved to −60 mesh. For most of the rock/water interaction experiments that used Tpt-FR, this −60 mesh material was pre-treated to remove the readily soluble component in a manner described in Oversby and Knauss (1983).

Petrographic Description

Much previous work has been done on the petrography of the Tpt. Detailed descriptions have been published for thin sections from outcrop (Lipman et al., 1966) and from many of the drillholes from the NNWSI program: J-13 (Heiken and Bevier, 1979), UE-25a#1 (Sykes et al., 1979; Carroll et al., 1981), USW G-1 (Bish et al., 1981), and USW G-2 and UE-25b#1h (Caporuscio et al., 1982; Broxton et al., 1982). This section relates the general petrographic characteristics of the Tpt-FR material, which will help locate the relative stratigraphic position of this outcrop with respect to the proposed repository horizon.

A detailed point count of this crystal-poor tuff was not made. Instead the general vitric texture and relative phenocryst proportions and nature will be described. Observations were made with transmitted light and a Leitz Orthoplan petrographic microscope; some SEM photos are included as well.

The Tpt-FR in thin section is densely to moderately welded, devitrified, and vapor-phase-altered. Phenocrysts make up less than 2% of the rock, and there is a slightly lesser amount (<1%) of voids. The bulk of the sample consists of the fine-grained devitrification products cristobalite, quartz, and alkali feldspar. In some areas coarse granophyric crystallization has produced sizable aggregates of interlocking quartz and alkali feldspar. Relict shards and pumice are easily recognized and frequently rimmed with clay or more opaque oxides.

Some of the vitric textures are illustrated in Figs. 11–19. A feathery, fluidal texture is developed in parts of the groundmass, outlined by clay or fine-grained oxides; bright spherulitic patches

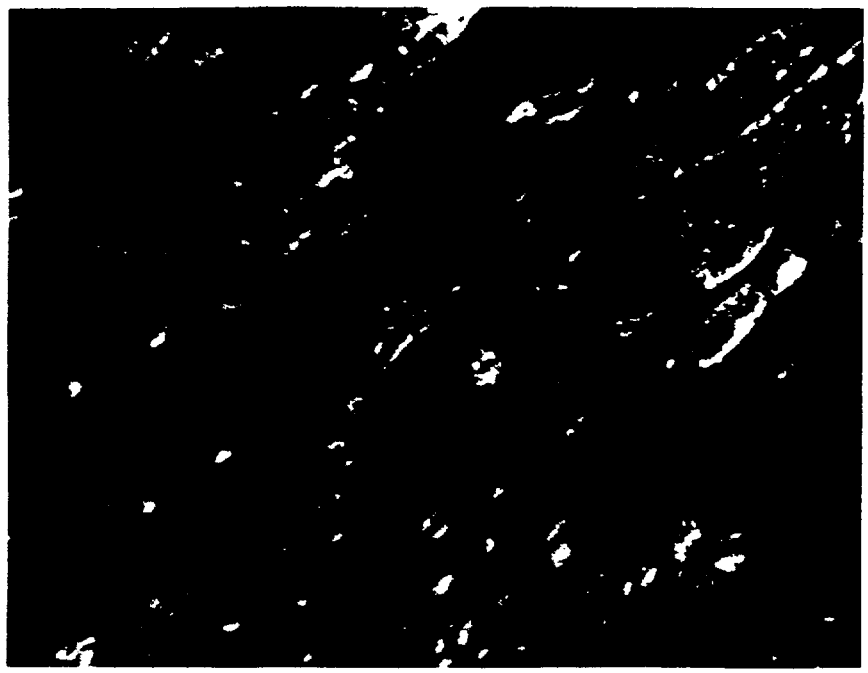

Figure 11. Spherulitic devitrification and fluidal vitric textures highlighted by clays, opaque oxides, or both.

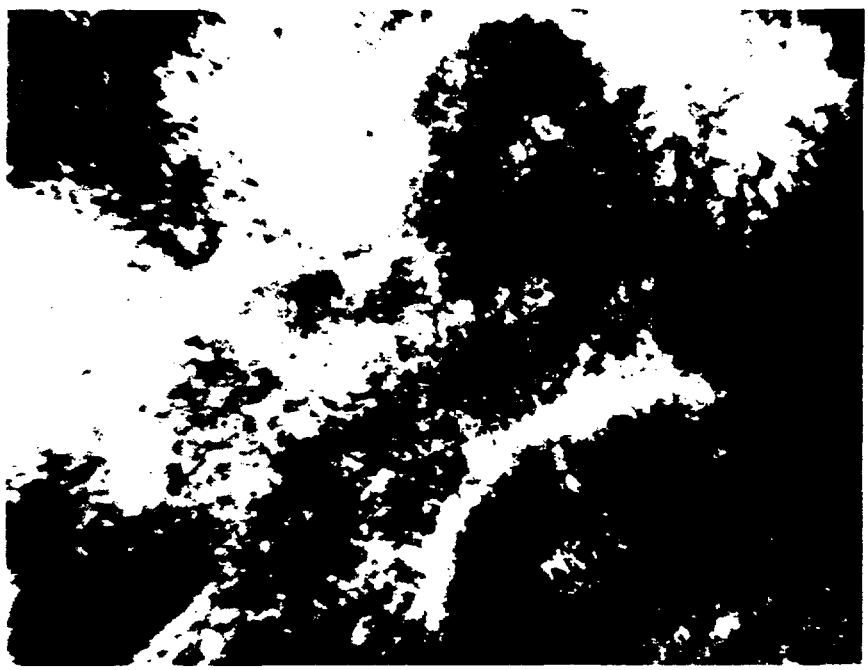

Figure 12. Dominant devitrification texture in groundmass is a coalescing pattern of fine-grained quartz, cristobalite, and alkali feldspar.

of silica are present (Fig. 11). The dominant devitrification texture in the groundmass is a coalescing pattern of fine-grained, radial, fibrous quartz and/or cristobalite and alkali feldspar (Fig. 12), or spherulites of the same minerals. These sprays frequently grow normal to, and are nucleated on the surfaces of, phenocrysts and relict pumice. The relict pumice tends to be filled with disseminated iron-oxides (Fig. 13), and the groundmass may show obvious flow texture around them (Fig. 14). Clay, oxides, or both also rim pumice, and spherulitic patches develop in their centers (Fig. 15). Within lithophysal cavities, minute acicular crystals of quartz and alkali feldspar radiate from the walls (Fig. 16). Within pumice a coarse, granophyric texture may also

Figure 13. Relict pumice rimmed by clay and filled with disseminated iron oxide.

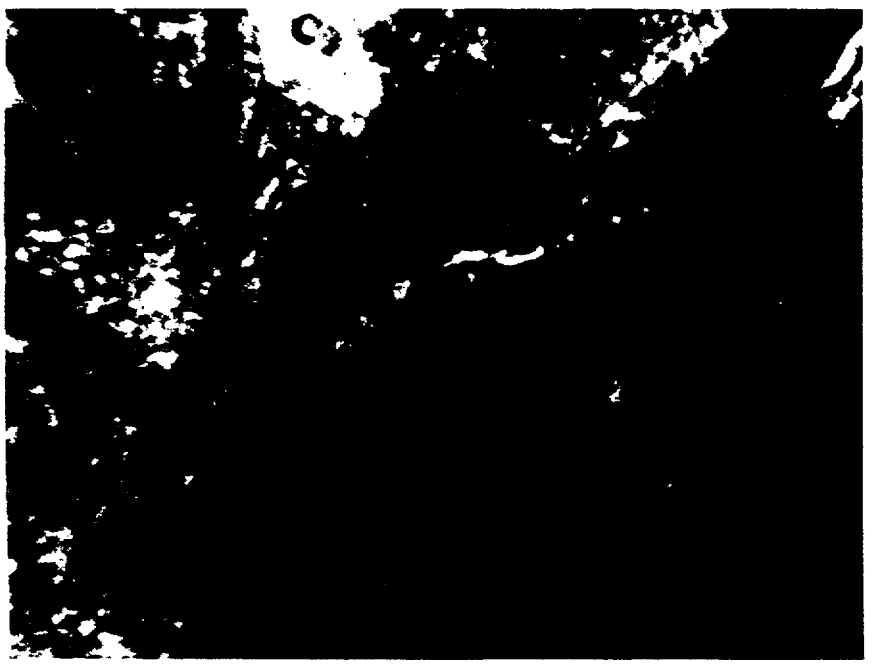

Figure 14. Flow evidenced in vitric texture around pumice.

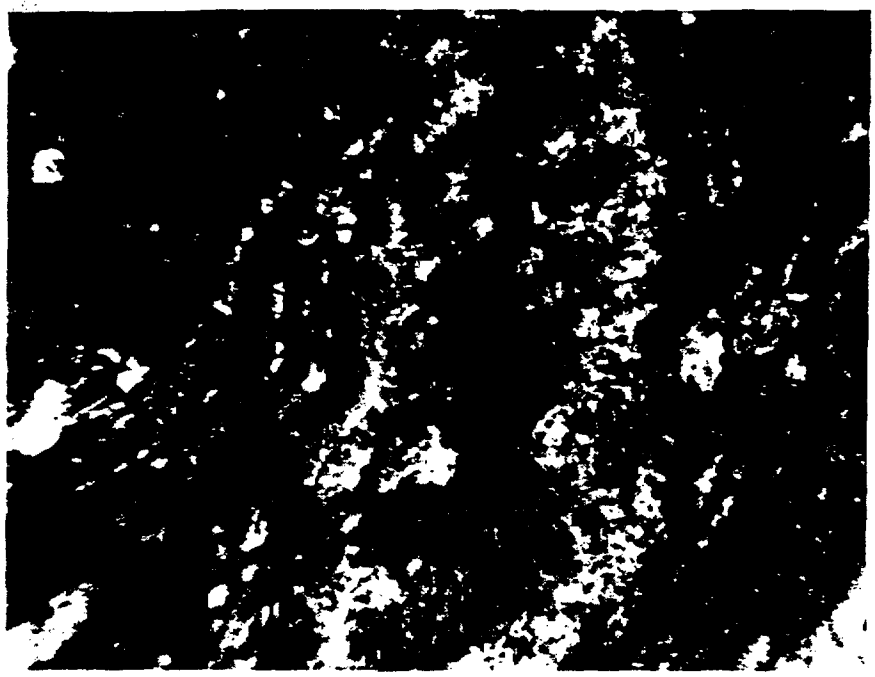

Figure 15. Clay, oxides, or both rimming pumice and spherulites developed in their centers.

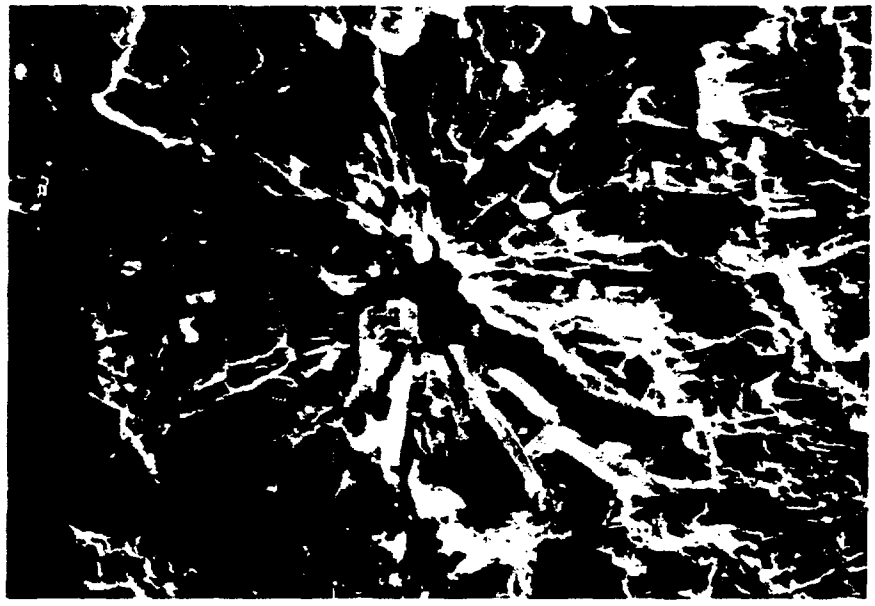

Figure 16. Acicular crystals of quartz and alkali feldspar radiate from the walls of lithophysal cavities.

develop, again consisting of quartz and alkali feldspar (Fig. 17). Examples of vapor-phase crystallization include terminated crystals of quartz, quartz after tridymite, and alkali feldspar growing in toward the center of the void space (Fig. 18). Vapor-phase effects are also seen in glass shards where axiolitic quartz and alkali feldspar bordering and perpendicular to the shard boundaries are capped by large, terminated, vapor-phase crystals that partly fill the void space (Fig. 19).

The vitric components just described make up more than 98% of the rock. The remainder of the rock consists of phenocrysts and lithic fragments of welded tuff or lava. The dominant phenocrysts are alkali feldspar (sanidine) and plagioclase (oligoclase to andesine); lesser blackened

Figure 17. Coarse, granophyric devitrification to quartz and alkali feldspar.

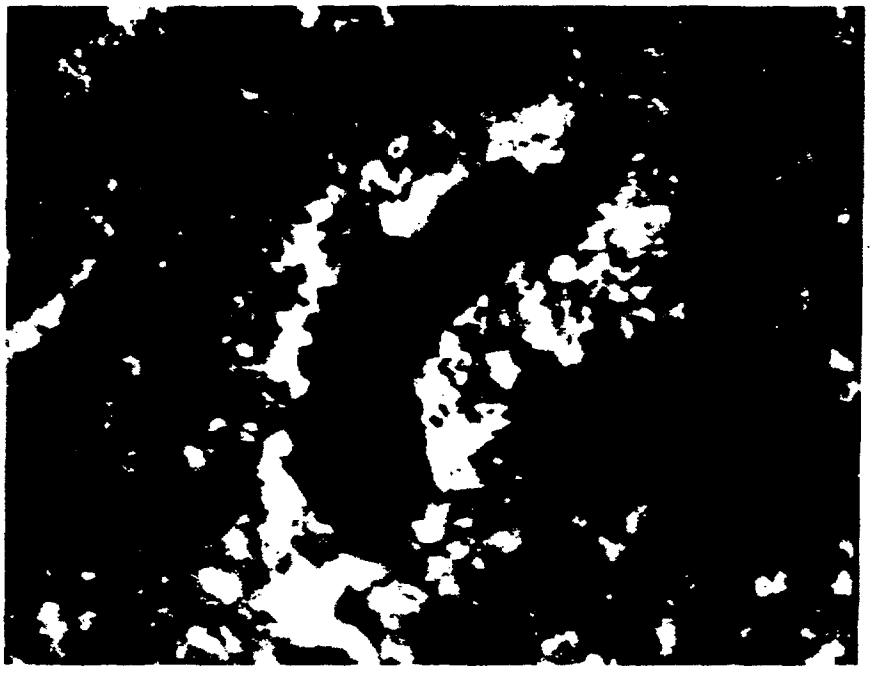

Figure 18. Terminated crystals of quartz, quartz after tridymite, and alkali feldspar result from vapor-phase deposition within voids.

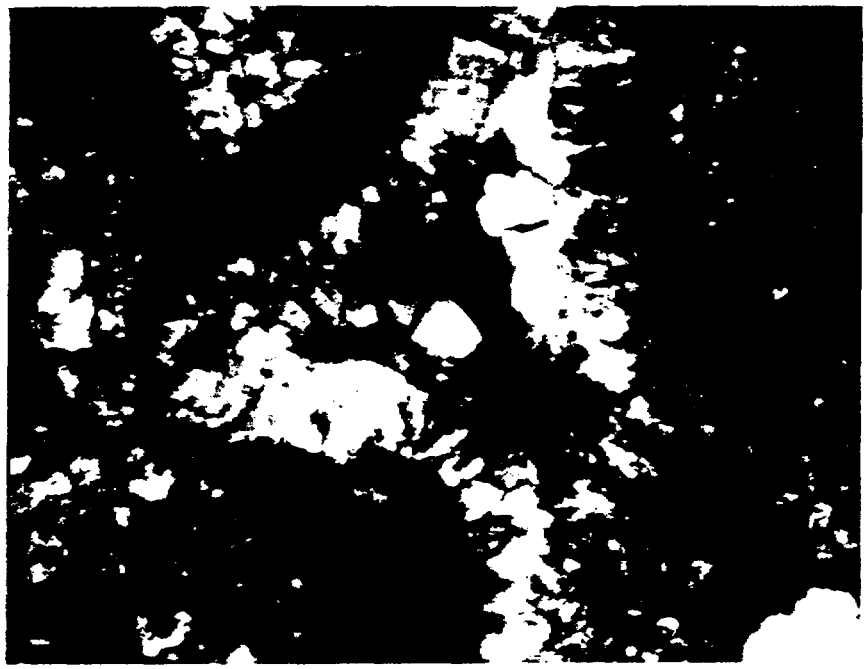

Figure 19. Axiolitic quartz and alkali feldspar perpendicular to and bordering shard boundaries are capped by large, terminated, vapor-phase crystals that partly fill the void space.

biotite; quartz and magnetite; and trace ilmenite and hornblende. Accessory minerals include zircon and apatite inclusions in the magnetite, ilmenite, and biotite. It is important to note that sanidine is more common than plagioclase.

Some observations follow on the phenocrysts and lithic fragments in Tpt-FR. Sanidine phenocrysts are euhedral to subhedral and not embayed (Fig. 20). The plagioclase is also euhedral to subhedral and may display normal or, less commonly, oscillatory zoning (Fig. 21). The biotite is smaller, blackened (Fig. 22), and altered to hematite (Fig. 23). The magnetite is usually (but not always) exsolved and frequently contains the accessories apatite and zircon (Fig. 24). One lithic fragment contained in the thin section examined was a flow-banded rhyolitic lava containing a plagioclase phenocryst that was compositionally indistinguishable from the plagioclase contained in the densely welded tuff (Fig. 25).

It is important to note that a large xenolith within the Tpt-FR thin section differed considerably from the rest of the rock (Fig. 26). Although devitrified, it was relatively crystal-rich and contained 10 to 15% phenocrysts. The phenocrysts were also quite different in appearance and composition. Most phenocrysts, particularly sanidine and quartz, were subhedral and embayed. Within this pumice, quartz was much more common than in the rest of the thin section, and the sanidine/plagioclase ratio was also higher.

This material resembles the description of the mixed pumice zone encountered by Lipman et al. (1966) in the upper parts of the densely welded, rhyolitic, crystal-poor Tpt at the Lathrop Wells section. Some pumice lapilli at that location more nearly resemble the crystal-rich, more mafic quartz-latite cap rock than they do the crystal-poor, rhyolitic tuff.

Most fractures encountered in thin section are nearly completely filled with iron-rich, manganese-rich (Fig. 27), or silicon-rich material. In some cases the fracture-filling material has served as the nucleus for coarse authigenic recrystallization.

This petrographic description provides some additional evidence on the relative stratigraphic position of Tpt-FR within the Tpt. The ratio of sanidine/plagioclase (>1) phenocrysts suggests a relatively high position within the densely welded, devitrified, and vapor-phase-altered Tpt. In other words, it would argue for placement in the densely welded interval between the two lithophysal zones beneath Yucca Mountain within the Tpt rather than between the lower lithophysal zone and the vitrophyre. Work in progress by Byers at Los Alamos (Vaniman, 1984) suggests that the most useful petrographic indicator of stratigraphic location within the lower Tpt is the distribution of brown microcrystalline devitrification intervals. Because this work has not yet been published, the petrographic criteria for location within the lower Tpt have not been applied to the

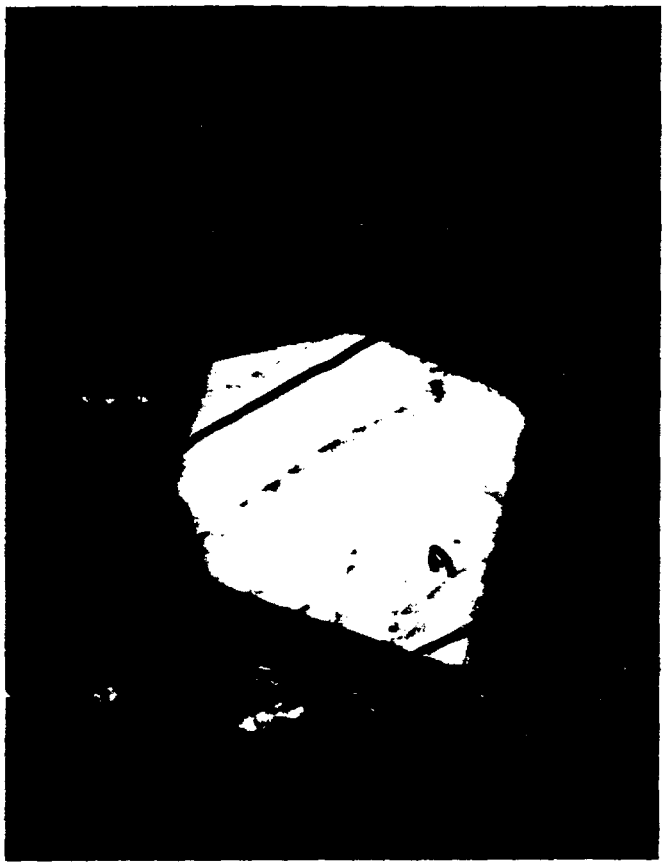

Figure 20. Sanidine phenocryst.

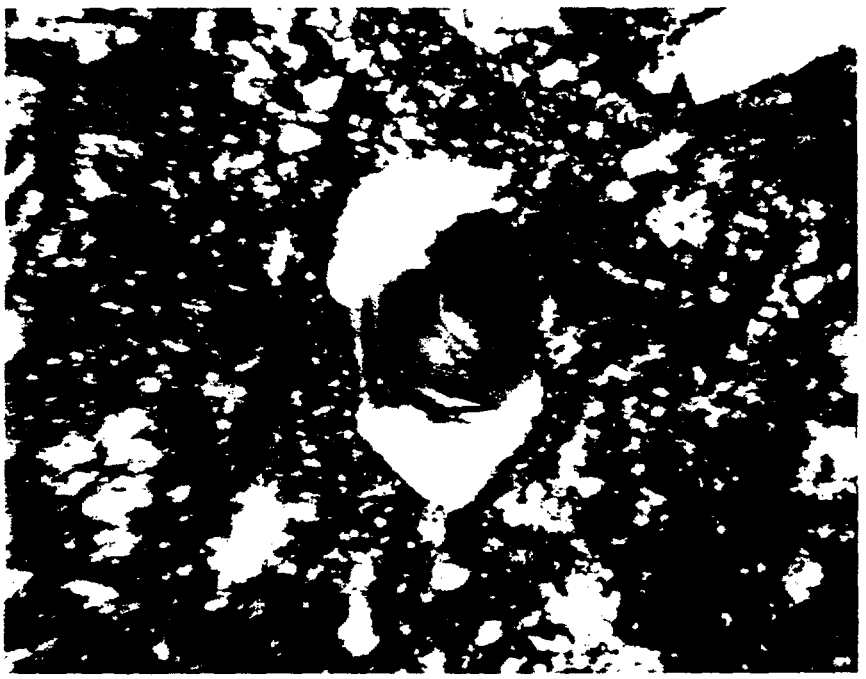

Figure 21. Plagioclase phenocryst displaying oscillatory zoning.

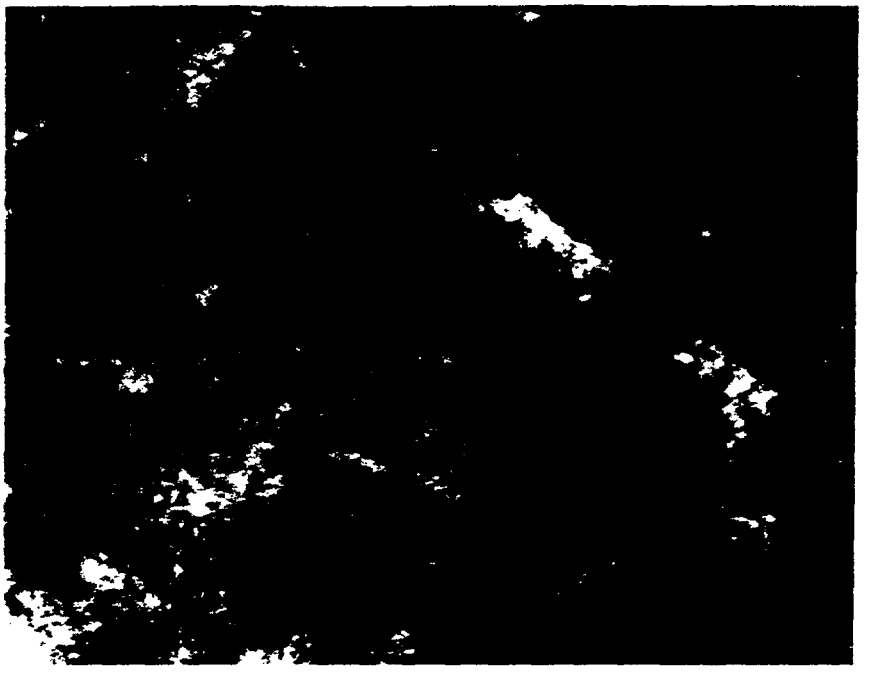

Figure 22. Blackened biotite.

Figure 23. Biotite altered to hematite.

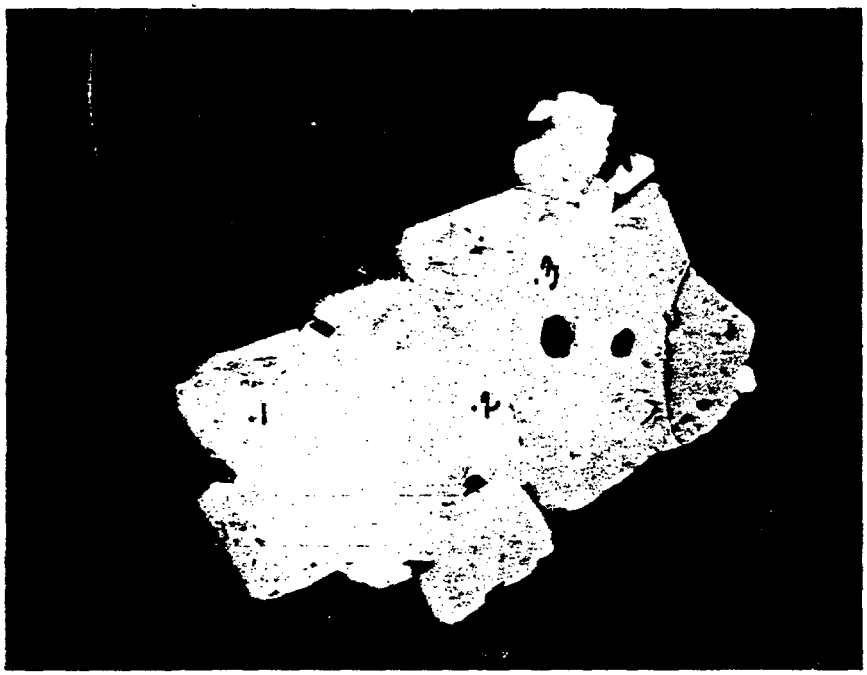

Figure 24. Non-exsolved magnetite with accessory zircon and apatite.

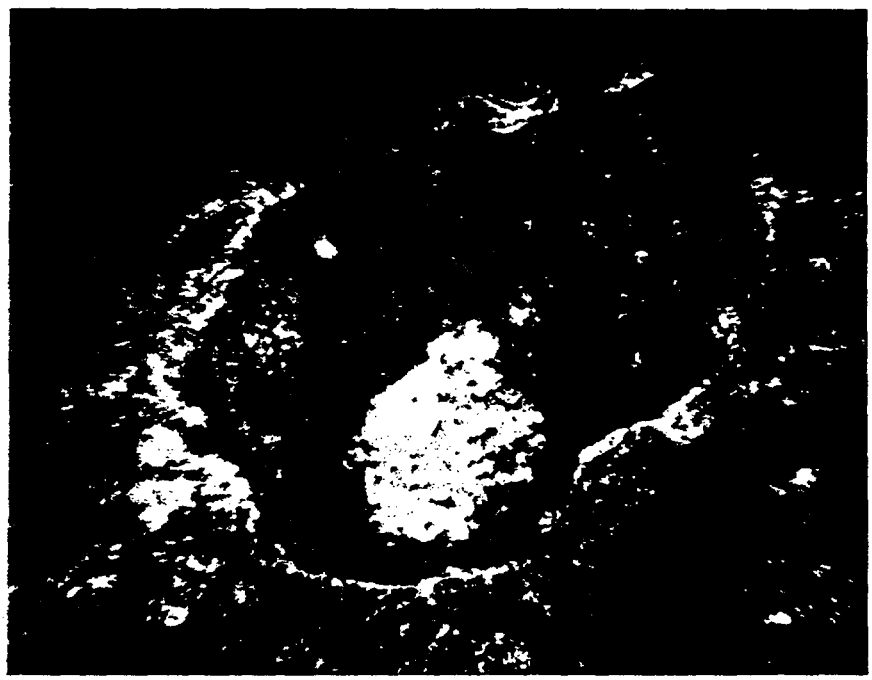

Figure 25. Lithic fragment of flow-banded rhyolitic lava.

Figure 26. Phenocrysts within the crystal-rich xenolith.

Figure 27. Fracture healed with manganese-rich and silicon-rich material.

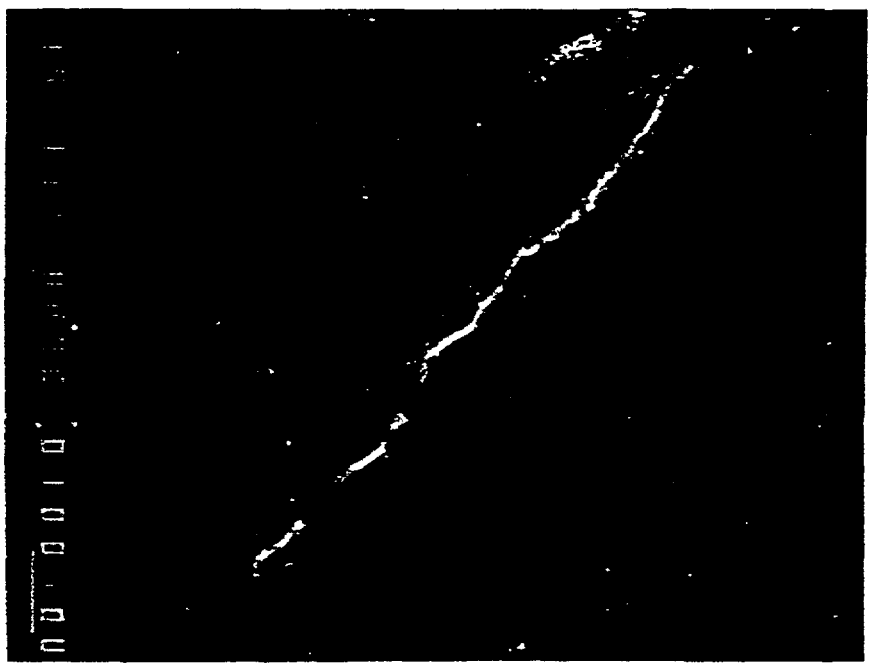

Tpt-FR thin section. It is not known whether the criteria developed for the Tpt beneath Yucca Mountain are also applicable to the unit for other locations where the Tpt is thinner (e.g., Busted Butte).

Bulk Mineralogy via XRD

X-ray diffraction (XRD) is a primary tool used to determine the mineralogic variability in the tuff units beneath Yucca Mountain. Bish and co-workers at Los Alamos have used quantitative XRD quite successfully for this purpose, and many of the aforementioned reports contain results of their analyses. A recently quantified XRD system at LLNL has been used to characterize the bulk mineralogy of Tpt-FR. Two samples of Tpt-FR were run for this purpose: a hand sample and a split of the prepared Tpt-FR that was crushed and sieved to −60 mesh. Both samples were ground and sieved to −325 mesh.

The sample powders were run on an automated powder diffractometer with theta-theta compensation to reduce low-angle background. Spectra were generated using Cu-K_α radiation and computerized data recording from 2° to 55° 2θ. The spectra were analyzed by computer for peak identification and calculation of d-spacing, relative intensity, and peak area. A quantitative analysis was then done with calibration based on mixtures of pure mineral standards diluted with quartz. As might be expected, the spectra, peaks identified, and the quantitative XRD results were essentially identical for the two samples. For the discussion to follow only the crushed sample results will be presented.

Figure 28 shows the XRD spectra, and Table 1 lists the derived peaks. The mineral phases that can be unambiguously identified are quartz, cristobalite, and alkali feldspar. Comparison with

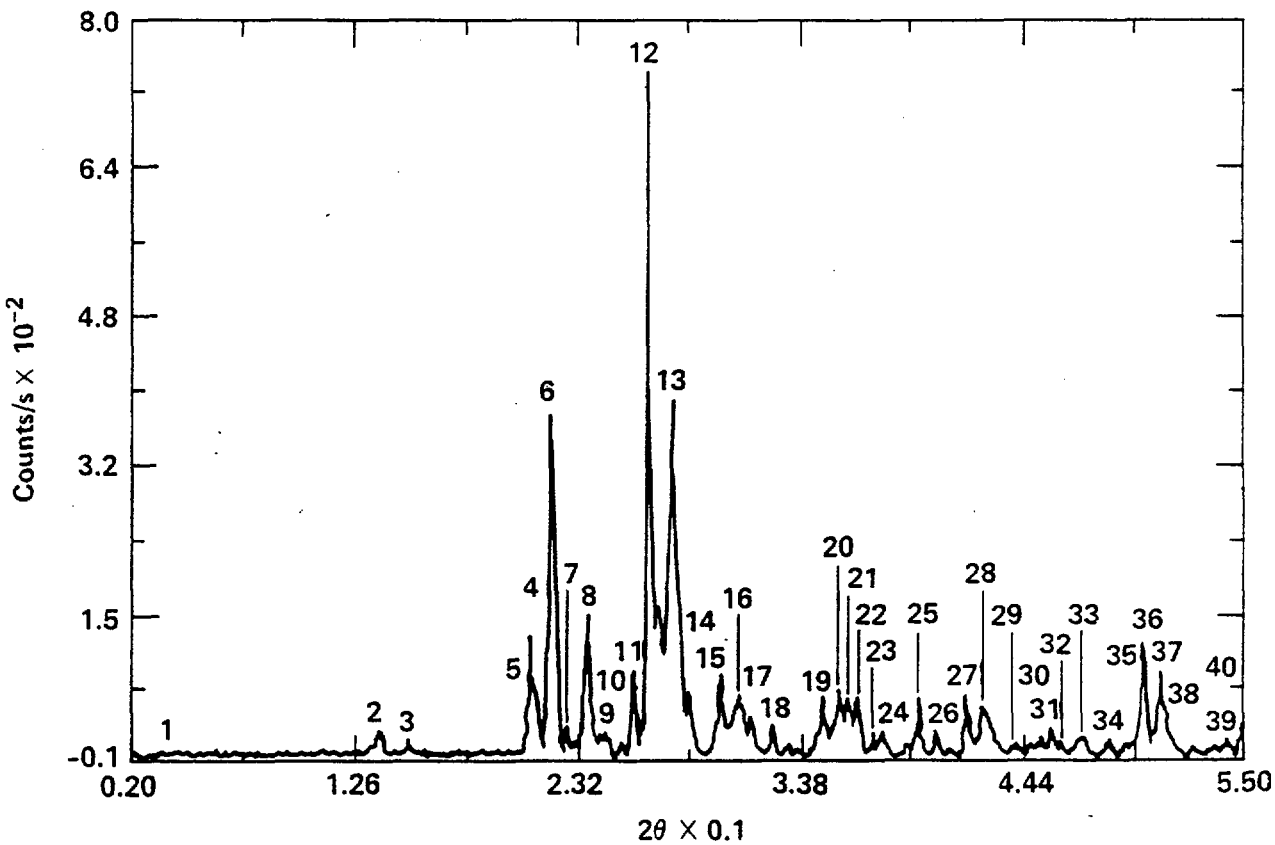

Figure 28. XRD spectra of Tpt-FR with the peaks numbered in Table 1.

Table 1. X-ray diffraction peaks identified by computer in the Topopah Spring Member tuff from Fran Ridge. Phases present include quartz, cristobalite, and alkali feldspar. Notably absent are peaks for zeolite, tridymite, and glass.

Peak No.	2θ	D-space	Height	Area
1	3.44	25.634	5	1.2
2	13.76	6.428	27	10.5
3	15.20	5.822	16	3.2
4	20.88	4.251	133	37.1
5	21.12	4.203	69	12.8
6	21.96	4.044	372	107.4
7	22.64	3.924	31	6.8
8	23.60	3.767	158	45.2
9	24.69	3.603	21	7.2
10	25.24	3.525	12	1.8
11	25.80	3.450	93	24.9
12	26.64	3.344	745	154.9
13	27.76	3.211	386	129.8
14	28.44	3.136	67	15.9
15	29.96	2.980	87	24.8
16	30.88	2.893	68	32.1
17	31.40	2.847	41	12.8
18	32.48	2.754	32	7.0
19	34.88	2.570	63	15.4
20	35.60	2.520	73	21.0
21	36.08	2.487	64	21.7
22	36.56	2.456	63	20.9
23	37.24	2.412	24	6.7
24	37.84	2.375	27	9.9
25	39.48	2.281	62	18.7
26	40.28	2.237	25	7.5
27	41.72	2.163	65	13.9
28	42.48	2.126	55	18.7
29	44.00	2.056	11	3.5
30	45.24	2.003	18	2.7
31	45.76	1.981	30	8.0
32	46.24	1.962	14	4.1
33	47.32	1.919	21	7.2
34	48.56	1.873	16	4.0
35	49.40	1.843	15	3.8
36	50.12	1.819	128	41.2
37	51.00	1.789	93	32.3
38	52.56	1.740	8	1.8
39	53.69	1.706	12	2.9
40	54.20	1.691	17	5.6

JCPDS cards shows the alkali feldspar peaks to be compatible with those of sanidine. The quantitative analysis made on these spectra suggests the proportions of the dominant mineral phases are 42% quartz, 29% cristobalite, and 29% feldspar. Although in thin sections clays were seen rimming pumice and disseminated throughout the matrix, no clearly discernible clay peak is seen in the spectra. This would suggest that clay is present at a few percent or less. It is also important to note that no peaks were identified for zeolites or tridymite, and no broad hump for glass was seen.

Bish et al. (1984) summarized the distribution of minerals within the repository horizon throughout the exploration block. They determined that there is little mineralogic variation within the moderately to densely welded Tpt repository horizon. Quartz, cristobalite, and alkali feldspar abundances have average values that fall within one standard deviation of each other. Within the entire Tpt the only major variation is the transition from tridymite to quartz with increasing depth. Tridymite is abundant in the upper Tpt, but generally absent below the zone of abundant lithophysae. The XRD data presented here, when compared with the figure of mineral distribution within the exploratory block given in Bish et al. (1984), suggest that the outcrop location is stratigraphically equivalent to a position below the zone of abundant lithophysae. The XRD data alone are not sufficient to determine whether or not Tpt-FR is equivalent to a position between the two lithophysal zones beneath Yucca Mountain or between the lowermost lithophysal zone and the vitrophyre. On the basis of the XRD identification of abundant quartz and cristobalite and the absence of tridymite, it can be said that Tpt-FR is below the uppermost lithophysal zone.

Bulk Chemistry via NAA

A sample of the cleaned, slabbed Tpt-FR was analyzed by NAA for a suite of elements. The material for this analysis was pulverized in a flat plate grinder with high-purity alumina plates and sieved to −140 mesh. A 200-mg split was mixed with an equal amount of Avicel binder and pelletized. The pellet was irradiated for 72 min at a flux of 1.9×10^{13} n/cm^2 s. After cooling times of 4.8, 12.9, and 31.9 d, the sample was counted with an automated Ge(Li) gamma spectrometer for periods of 8,000, 20,000, and 20,000 s, respectively. Nuclide identification and data reduction for multiple counts for each element were done with the GAMANAL, NADAC, and MERGE computer programs (Gunnink and Niday, 1972; Heft and Martin, 1977). The USGS standard rock G2 was used as a check standard for each irradiation.

Table 2 summarizes the data obtained from the NAA analyses. Because of the long delay before the first count period, no elements with short-lived activation products (e.g., silicon or aluminum) are detected. Fortunately these major elements are easily detected by electron microprobe analysis; see page 21 for a discussion of these results. Few minor and trace element analyses have been published, but the semiquantitative analyses based on emission spectrometry from Lipman et al. (1966) do agree reasonably well—even though the detection limits for the emission spectrometry are considerably worse in many cases.

It should be noted that NAA and EMP were used to analyze samples from the proposed repository depth at the following locations: several holes (USW G-1, USW GU-3, and USW G-4) within the exploration block, the horizontal hole (UE-25h#1) at Fran Ridge, and the Busted Butte type section. (These analyses were made as part of a study to document the near-field variation in bulk chemistry and individual mineral composition expected in the repository.) Although the NAA analyses are complete, the data will be the subject of a short topical report at a later date and will not be presented here. The results of the Tpt-FR NAA analyses shown in Table 2 agree with those taken from the actual repository depth beneath Yucca Mountain, which will be reported later (Knauss, 1984, in preparation).

Table 2. Results for neutron activation analysis of Tpt-FR.

Element	ppm
Na	$2.809 \pm 0.087 \times 10^4$
K	$3.931 \pm 0.354 \times 10^4$
Ca	$0.902 \pm 0.116 \times 10^4$
Fe	$0.621 \pm 0.009 \times 10^4$
Sc	2.257 ± 0.019
Cr	1.548 ± 0.998
Co	0.164 ± 0.026
Ni	Not detectable
Zn	42.88 ± 2.97
Ga	Not detectable
As	4.609 ± 1.005
Rb	187.8 ± 2.8
Sr	Not detectable
Zr	153.6 ± 25.5
Mo	24.00 ± 5.78
Ag	Not detectable
Sb	0.333 ± 0.035
Cs	3.821 ± 0.081
Ba	52.56 ± 14.24
La	35.76 ± 0.38
Ce	65.47 ± 0.86
Nd	30.88 ± 4.82
Sm	5.900 ± 0.133
Eu	0.275 ± 0.018
Gd	6.921 ± 3.084
Tb	0.768 ± 0.018
Yb	3.014 ± 0.067
Lu	0.518 ± 0.014
Hf	4.991 ± 0.081
Ta	1.331 ± 0.031
W	Not detectable
Au	Not detectable
Th	22.10 ± 0.15
U	4.274 ± 0.197

Table 3. Results of quantitative wavelength dispersive spectrometry (WDS) analysis of polished thin sections of Tpt-FR samples. Oxide weight percentages were calculated using a Bence-Albee correction scheme.

Table 3a. Sanidine.

Oxide	Ph2A Pt1	Ph2B Pt1	Ph2B Pt2	Ph4A Pt1	Ph5A Pt1	Ph5B Pt1	Ph5C Pt1	Ph9A[a] Pt1
SiO_2	67.80	65.67	67.96	68.31	67.84	66.11	66.70	66.71
Al_2O_3	19.71	19.44	19.88	19.67	19.12	19.17	19.47	20.39
K_2O	8.57	8.82	8.59	8.00	8.88	8.86	8.80	9.14
Na_2O	5.18	5.14	5.08	5.79	5.14	5.34	5.21	5.11
CaO	0.37	0.33	0.33	0.50	0.37	0.41	0.36	0.39
MgO	0.03	0.00	0.00	0.03	0.03	0.05	0.05	0.02
TiO_2	0.00	0.05	0.09	0.10	0.00	0.08	0.00	0.06
FeO	0.04	0.13	0.12	0.14	0.03	0.06	0.05	0.00
BaO	0.00	0.00	0.20	0.00	0.00	0.15	0.00	0.00
Total	101.70	99.59	102.25	102.54	101.41	100.22	100.63	101.80
QZ	–	–	–	–	–	–	–	–
OR	51.21	52.20	51.83	46.51	52.31	51.24	51.76	53.11
AB	46.94	46.15	46.49	51.05	45.88	46.78	46.49	45.01
AN	1.85	1.66	1.68	2.45	1.81	1.98	1.75	1.88

Oxide	Ph9B Pt1	Ph10A Pt1	Ph11A Pt1	Ph13D Pt1	Ph14B Pt1	Ph14C Pt1	Ph18A Pt1	Ph23A[a] Pt1
SiO_2	67.67	67.25	67.63	66.85	68.75	67.01	66.38	67.50
Al_2O_3	19.87	20.08	18.87	20.03	17.90	19.67	19.28	19.62
K_2O	10.28	10.15	10.77	9.49	8.62	10.08	10.16	9.60
Na_2O	4.20	4.04	4.00	5.03	3.73	4.41	4.39	4.58
CaO	0.18	0.27	0.08	0.35	0.27	0.28	0.30	0.34
MgO	0.00	0.00	0.02	0.00	0.00	0.00	0.03	0.00
TiO_2	0.00	0.02	0.00	0.09	0.09	0.00	0.05	0.00
FeO	0.12	0.05	0.00	0.15	0.22	0.26	0.10	0.08
BaO	0.00	0.15	0.00	0.09	0.00	0.00	0.00	0.00
Total	102.32	102.01	101.37	102.08	99.58	101.70	100.71	101.74
QZ	–	–	–	–	–	–	–	–
OR	61.22	61.52	63.75	54.50	59.45	59.27	59.55	57.04
AB	37.89	37.14	35.86	43.82	38.99	39.35	38.98	41.24
AN	0.89	1.35	0.39	1.68	1.56	1.38	1.47	1.72

[a] Ph = *photo number*, A–D = *phenocryst number*, and Pt = *point number*.

Surface Area of Crushed Tuff

The surface areas of the crushed tuff (split Tpt-FR A2) and the solid core wafers were determined with the BET gas adsorption method. The argon gas adsorption method was used because of its better detection limits. A Micrometrics ORR surface-area analyzer was used for this purpose. The results for the crushed tuff (−60 mesh) are summarized below:

Tpt-FR (A)	0.928 m^2/g
Tpt-FR (B)	1.058 m^2/g
Tpt-FR (C)	1.476 m^2/g
Average	1.154 +/− 0.286 m^2/g

The results for the core wafers will be presented in a later report, which will summarize results of hydrothermal rock/water interaction tests that were run with Tpt-FR core wafers and J-13 water at 150°C in static Parr bombs. It should be noted that the polished core wafers of Tpt-FR had a significantly lower specific surface area than the crushed tuff, which differs from the surface area comparison between similarly treated Bullfrog Member Tuff (Knauss, 1983). The Bullfrog had considerable interconnected porosity, whereas the Tpt-FR pores are much less interconnected.

Individual Mineral Phase Chemistry via EMP

After waste emplacement, the aqueous environment surrounding the waste package will be determined by the complex interaction between solid and liquid phases. The composition of the resulting solution will depend on the chemistry of the individual minerals present, the rate at which they dissolve, and the rate at which secondary minerals precipitate, and not simply on the whole rock chemistry and initial solution chemistry. This necessitates a knowledge of the composition of these individual mineral phases. This information is also needed to fully understand the sources and sinks for dissolved species and to model the evolution of the solution composition through time.

For geochemical characterization of the individual mineral phases present in the Tpt-FR samples, a polished thin section and two polished core wafers were examined by SEM, analyzed by quantitative WDS, and analyzed by semiquantitative EDS with a fully automated EMP equipped with beam stabilization. For both EDS and WDS analysis the JEOL 733 Superprobe was typically operated at a 15-kV accelerating voltage, a 15-nA (or less) beam current, and a rastered beam of from 10 to 100 μm^2, depending on the size of the object under study. A point beam was used for EDS analysis of small phases. To minimize volatile loss, sodium and potassium were always counted first, and the beam was automatically blanked during large spectrometer rotations. To minimize spectrometer rotation time, and hence counting time on the sample, the order of analysis for the remaining elements was also computer-determined. The elemental analyses were calibrated against appropriate well-characterized silicate mineral standards obtained from the Charles Taylor Co., Palo Alto, CA. The oxide weight percentages reported in the tables were calculated with a Bence-Albee correction scheme (Bence and Albee, 1968).

Table 3 shows the results of quantitative WDS analysis for the polished thin section, grouped by phase. The results of similar analyses made on two polished core wafers of Tpt-FR are shown in Tables 4 and 5. Note that pumice or matrix data are analyses of a mixture of phases (quartz and alkali feldspar) on a micrometer to submicrometer scale. Phenocryst analyses are at their cores, at mid-range between core and rim, or both, unless otherwise noted. In addition to analyses of the dominant mineral phases present as phenocrysts (alkali feldspar, plagioclase, biotite, magnetite, ilmenite, and quartz), some analyses of the accessory minerals zircon and apatite are also included.

Histograms have been made to show the dominant composition and range in composition for the primary mineral phases present as phenocrysts in Tpt-FR. As was established with the Bullfrog Member Tuff, the analytical results obtained from a polished core wafer or a polished thin section of the same samples are indistinguishable, if proper care is taken in the sample preparation (Knauss, 1983). Both ordinary histograms and cumulative frequency plots were made for the phases alkali feldspar, plagioclase, and biotite, which together with magnetite and ilmenite are the dominant phenocrysts present in Tpt-FR.

Table 3c. Pumice/quartz matrix.

Oxide	Ph25D Pt1	Ph7B Pt1	Ph26E Pt1	Ph11B[a] Pt1
SiO_2	79.86	99.28	89.94	80.18
Al_2O_3	11.74	0.04	4.66	10.93
K_2O	0.63	0.00	1.17	3.33
Na_2O	4.94	0.03	1.74	3.40
CaO	1.16	0.00	0.30	0.66
MgO	0.05	0.00	0.06	0.00
TiO_2	0.00	0.10	0.03	0.03
FeO	0.16	0.00	0.10	0.52
MnO	0.00	–	0.08	0.05
BaO	0.00	0.37	0.39	0.00
Total	98.54	99.82	98.47	99.10
QZ	44.27	100.00	74.75	45.36
OR	3.84	–	7.52	20.83
AB	45.91	–	16.97	32.29
AN	5.97	–	0.76	2.55

[a]Ph = photo number, A–E = phenocryst number, and Pt = point number.

Table 3d. Magnetite.

Oxide	Ph19A Pt1	Ph21C Pt1	Ph21E Pt1	Ph21D Pt1	Ph24A[a] Pt1
SiO_2	0.32	0.00	0.28	0.65	0.00
Al_2O_3	0.70	1.89	1.61	2.56	1.39
K_2O	–	–	–	–	–
Na_2O	–	–	–	–	–
CaO	–	–	–	–	–
MgO	0.05	0.00	0.00	0.00	0.08
TiO_2	19.08	5.19	5.77	4.41	6.19
FeO	70.71	82.42	83.15	82.72	83.03
MnO	2.59	1.17	1.15	0.83	1.82
F	–	–	–	–	–
Cl	–	–	–	–	–
Total	93.45	90.67	91.96	91.17	92.57
Ti/Fe	0.243	0.057	0.062	0.048	0.067
Mg/Mg+Fe	0.001	0.000	0.000	0.000	0.002
Ulvospinel	0.448	0.143	0.160	0.126	0.161
Magnetite	0.552	0.857	0.840	0.874	0.839

[a]Ph = photo number, A–E = phenocryst number, and Pt = point number.

Table 3e. Biotite.

Oxide	Ph16A Pt1	Ph16A Pt2	Ph16A Pt4	Ph16A[a] Pt5
SiO_2	33.31	33.53	33.10	32.89
Al_2O_3	12.23	12.40	12.47	11.85
K_2O	7.96	8.18	8.07	7.68
Na_2O	0.42	0.46	0.47	0.46
CaO	0.00	0.06	0.05	0.00
FeO	29.89	28.83	29.26	32.79
MgO	9.13	9.42	8.85	8.90
MnO	0.80	–	–	–
TiO_2	4.15	4.06	3.83	3.99
F	0.00	–	–	–
Cl	0.15	–	–	–
Total	98.05	96.94	96.10	98.56
Ti/Fe	0.125	0.127	0.118	0.110
Mg/Mg+Fe	0.355	0.370	0.353	0.328

[a]Ph = photo number, A = phenocryst number, and Pt = point number.

Table 3f. Ilmenite.

Oxide	Ph188 Pt1[a]
SiO_2	0.22
Al_2O_3	0.06
K_2O	–
Na_2O	–
CaO	–
FeO	47.31
MgO	0.24
MnO	3.40
TiO_2	48.59
F	–
Cl	–
Total	99.81
Ti/Fe	0.924
Mg/Mg+Fe	0.009
Ilmenite	0.915
Hematite	0.085

[a]Ph = photo number, Pt = point number.

Table 3b. Plagioclase.

Oxide	Ph1A Pt1	Ph7A Pt1	Ph14A Pt1	Ph15A Pt1	Ph15B Pt1	Ph20A Pt1	Ph20A[a] Pt2
SiO_2	65.96	60.38	62.48	64.39	63.59	61.94	63.08
Al_2O_3	21.95	26.51	22.75	22.70	23.43	23.45	23.26
K_2O	1.10	0.42	0.81	1.38	1.07	1.08	1.12
Na_2O	9.18	6.52	8.39	8.39	8.54	8.42	8.43
CaO	2.63	7.97	5.31	3.58	3.81	3.74	3.78
MgO	0.00	0.00	0.05	0.03	0.00	0.02	0.00
TiO_2	0.00	0.12	0.10	0.10	0.01	0.07	0.00
FeO	0.18	0.04	0.15	0.13	0.16	0.12	0.15
BaO	0.00	0.00	0.00	0.00	0.00	0.00	0.18
Total	101.01	101.97	100.04	100.70	100.61	98.84	100.00
QZ	–	–	–	–	–	–	–
OR	6.37	2.47	4.50	8.05	6.19	6.36	6.55
AB	80.83	58.16	70.72	74.38	75.22	75.19	74.85
AN	12.80	39.37	24.79	17.57	18.59	18.46	18.60

Oxide	Ph22A Pt1	Ph22A Pt2	Ph26A Pt1	Ph26F Pt1	Ph27A Pt1	Ph27A Pt2	Ph29B[a] Pt1
SiO_2	64.65	63.33	64.23	61.93	59.85	55.89	57.80
Al_2O_3	22.95	23.13	22.79	25.13	26.27	27.69	28.29
K_2O	1.15	1.32	1.15	0.67	0.50	0.41	0.40
Na_2O	8.42	8.41	8.55	7.72	6.64	6.51	5.92
CaO	3.45	3.44	3.43	5.89	7.30	8.25	9.28
MgO	0.04	0.00	0.02	0.00	0.06	0.00	0.03
TiO_2	0.09	0.00	0.00	0.02	0.11	0.00	0.06
FeO	0.08	0.15	0.11	0.09	0.16	0.11	0.27
BaO	0.00	0.38	0.00	0.00	0.00	0.44	0.00
Total	100.84	100.15	100.29	101.44	100.88	99.31	102.06
QZ	–	–	–	–	–	–	–
OR	6.85	7.78	6.79	3.86	2.98	2.40	2.33
AB	75.93	75.21	76.27	67.59	60.33	57.36	52.29
AN	17.23	17.01	16.94	28.55	36.70	40.25	45.39

[a] Ph = photo number, A-F = phenocryst number, and Pt = point number.

Table 4. Results of quantitative electron microprobe analyses of phases contained in the polished core wafer Tpt CWO_3. Oxide weight percentages were calculated using a Bence-Albee correction scheme.

Table 4a. Sanidine.

Oxide	Ph6 Pt1	Ph6 Pt2	Ph7 Pt1	Ph7 Pt2	Ph7 Pt3	Ph8 Pt1	Ph8 Pt2	Ph8 Pt3	Ph9 Pt1	Ph9 Pt2	Ph9 Pt3	Ph9 Pt4	Ph10 Pt1	Ph10[a] Pt2
SiO_2	68.54	68.05	66.48	65.09	67.26	68.33	66.92	66.06	67.48	66.35	64.70	65.65	67.60	66.40
Al_2O_3	19.08	18.94	20.27	19.33	19.66	19.28	20.02	18.40	19.10	19.01	18.23	20.10	19.60	18.35
K_2O	9.78	8.61	9.65	9.05	9.08	9.87	10.19	10.14	10.22	10.38	9.98	8.09	8.54	9.56
Na_2O	4.15	4.99	5.01	5.10	5.06	4.36	4.45	4.38	3.99	4.13	4.35	5.92	4.77	4.58
CaO	0.22	0.22	0.31	0.31	0.31	0.11	0.11	0.11	0.19	0.19	0.19	0.59	0.33	0.33
MgO	0.00	0.00	0.00	0.00	0.00	0.00	0.00	0.00	0.00	0.00	0.00	0.00	0.00	0.00
TiO_2	0.00	0.04	0.00	0.03	0.00	0.04	0.00	0.06	0.00	0.00	0.02	0.00	0.00	0.07
FeO	0.17	0.10	0.12	0.12	0.13	0.15	0.13	0.18	0.08	0.13	0.11	0.09	0.16	0.10
BaO	0.00	0.20	0.00	0.43	0.30	0.00	0.00	0.15	0.00	0.00	0.19	0.12	0.00	0.17
Total	101.94	101.16	101.83	99.46	101.80	102.15	101.82	99.47	101.05	100.18	97.77	100.56	101.00	99.55
QZ	–	–	–	–	–	–	–	–	–	–	–	–	–	–
OR	60.28	52.61	55.19	53.11	53.44	59.60	59.87	60.07	62.37	61.89	59.65	46.07	53.30	56.97
AB	38.59	46.27	44.05	45.37	45.81	40.12	39.85	39.37	37.17	37.64	39.41	51.09	45.88	41.39
AN	1.13	1.13	0.76	1.52	0.76	0.28	0.28	0.56	0.46	0.47	0.93	2.84	0.82	1.64

Oxide	Ph12 Pt1	Ph13 Pt1	Ph13 Pt2	Ph13 Pt3	Ph18 Pt1	Ph18 Pt1	Ph18 Pt3	Ph18 Pt4	Ph32 Pt1	Ph32 Pt2	Ph32 Pt3	Ph35 Pt1	Ph35 Pt2	Ph35[a] Pt3
SiO_2	64.96	66.49	68.17	66.27	66.53	68.37	66.22	66.00	66.49	65.37	65.75	67.41	67.47	65.10
Al_2O_3	19.13	19.04	18.95	18.62	19.13	19.13	19.71	18.47	19.61	20.07	18.88	19.34	19.56	18.92
K_2O	9.22	10.33	9.80	10.63	10.10	10.37	10.01	9.93	10.19	10.38	9.83	9.85	9.88	9.84
Na_2O	5.09	4.18	4.35	4.01	4.39	4.36	4.58	4.55	4.39	4.46	4.57	4.38	4.37	4.71
CaO	0.39	0.10	0.10	0.10	0.22	0.22	0.22	0.22	0.26	0.26	0.26	0.24	0.24	0.24
MgO	0.00	0.00	0.00	0.00	0.00	0.00	0.00	0.00	0.00	0.00	0.00	0.00	0.00	0.00
TiO_2	0.02	0.00	0.00	0.05	0.03	0.02	0.06	0.00	0.00	0.04	0.00	0.03	0.00	0.05
FeO	0.19	0.36	0.15	0.10	0.10	0.14	0.18	0.13	0.11	0.08	0.10	0.07	0.07	0.04
BaO	0.21	0.00	0.00	0.15	0.00	0.00	0.00	0.14	0.07	0.10	0.23	0.00	0.00	0.09
Total	99.22	100.50	101.52	99.95	100.50	100.61	100.99	99.43	101.12	100.76	99.62	101.31	101.59	99.00
QZ	–	–	–	–	–	–	–	–	–	–	–	–	–	–
OR	53.42	61.68	59.48	63.30	59.75	60.52	58.52	58.36	59.85	59.91	57.89	59.13	59.25	57.25
AB	44.67	38.06	40.26	36.18	39.72	38.95	40.95	40.57	39.50	39.44	40.81	40.27	40.15	41.55
AN	1.92	0.26	0.26	0.52	0.53	0.53	0.53	1.07	0.65	0.65	1.30	0.60	0.50	1.20

[a] Ph = photo number, Pt = point number.

Table 3g. Zircon.

Oxide	Ph21B Pt1[a]
SiO_2	31.52
Al_2O_3	0.03
K_2O	–
Na_2O	–
CaO	–
FeO	0.36
MgO	0.04
MnO	–
TiO_2	0.10
F	–
Cl	–
ZrO_2	64.35
Total	96.39

[a]Ph = photo number, B = phenocryst number, and Pt = point number.

Table 3h. Apatite.

Oxide	Ph21A Pt1[a]
SiO_2	1.26
Al_2O_3	–
K_2O	–
Na_2O	–
CaO	52.19
FeO	0.50
MgO	–
MnO	–
TiO_2	–
F	3.47
Cl	0.12
P_2O_5	40.15
Ce_2O_3	1.02
Total	98.71

[a]Ph = photo number, A = phenocryst number, and Pt = point number.

Table 4c. Magnetite.

Oxide	Ph1 Pt1	Ph1 Pt2	Ph1 Pt3	Ph2 Pt1	Ph2 Pt2	Ph3 Pt1	Ph3 Pt2	Ph3 Pt3	Ph3 Pt4	Ph21 Pt1	Ph21[a] Pt2
SiO_2	0.05	0.04	0.03	0.09	0.00	0.04	0.10	0.08	0.00	0.20	0.07
Al_2O_3	0.51	0.51	0.49	0.53	0.40	0.51	0.93	2.03	0.48	0.94	1.11
K_2O	–	–	–	–	–	–	–	–	–	–	–
Na_2O	–	–	–	–	–	–	–	–	–	–	–
CaO	–	–	–	–	–	–	–	–	–	–	–
FeO	75.05	75.49	76.42	75.42	73.99	77.13	89.96	89.12	76.12	85.98	87.01
MgO	0.04	0.08	0.00	0.04	0.05	0.06	0.00	0.04	0.04	0.30	0.13
MnO	0.92	0.70	0.69	0.74	0.51	0.80	0.40	0.15	0.59	3.00	2.22
TiO_2	16.10	16.94	15.66	14.57	16.20	14.16	0.47	0.24	15.85	1.81	1.64
F	–	–	–	–	–	–	–	–	–	–	–
Cl	–	–	–	–	–	–	–	–	–	–	–
Total	92.67	93.76	93.29	91.39	91.15	92.70	91.86	91.66	93.08	92.23	92.18
Ti/Fe	0.193	0.202	0.185	0.174	0.197	0.165	0.005	0.002	0.187	0.019	0.017
Mg/Mg+Fe	0.001	0.002	0.000	0.001	0.001	0.001	0.000	0.001	0.001	0.006	0.003
Ulvospinel	0.474	0.495	0.459	0.435	0.488	0.415	0.008	0.005	0.309	0.004	0.012
Magnetite	0.526	0.505	0.541	0.565	0.512	0.585	0.992	0.995	0.691	0.996	0.988

[a] Ph = photo number, Pt = point number.

Table 4d. Zircon.

Oxide	Ph24 Pt1[a]
SiO_2	31.73
Al_2O_3	0.00
K_2O	0.04
Na_2O	0.03
CaO	0.04
FeO	0.18
MgO	0.05
MnO	0.06
TiO_2	0.12
F	–
Cl	–
ZrO_2	65.79
Total	98.04

[a]Ph = photo number, Pt = point number.

Table 4b. Plagioclase.

Oxide	Ph12 Pt1	Ph12 Pt2	Ph12 Pt3	Ph12 Pt4	Ph28 Pt1	Ph28 Pt2	Ph37 Pt1	Ph37 Pt2	Ph37[a] Pt3
SiO_2	65.47	66.35	65.96	65.16	61.87	63.44	65.28	65.90	68.62
Al_2O_3	22.67	22.40	21.58	21.83	22.30	23.15	23.72	23.41	18.87
K_2O	1.09	1.47	1.23	1.25	0.68	0.67	1.26	1.28	0.83
Na_2O	8.93	9.16	9.10	8.95	8.38	8.74	8.59	8.73	7.62
CaO	2.84	2.63	2.50	2.65	3.98	3.99	3.59	3.48	2.54
MgO	0.00	0.00	0.00	0.00	0.14	0.02	0.00	0.00	0.00
TiO_2	0.00	0.04	0.00	0.00	0.00	0.08	0.00	0.08	0.03
FeO	0.20	0.16	0.24	0.04	0.48	0.32	0.23	0.12	0.06
BaO	0.00	0.00	0.04	0.02	0.00	0.00	0.00	0.08	0.00
Total	101.20	102.20	100.65	99.90	97.84	100.41	102.65	103.08	98.57
QZ	–	–	–	–	–	–	–	–	–
OR	6.39	8.35	7.17	7.34	4.06	3.89	7.27	7.35	5.69
AB	79.58	79.07	80.59	79.62	75.97	76.72	75.32	75.90	79.64
AN	14.02	12.57	12.24	13.04	19.97	19.40	17.41	16.74	14.67

Oxide	Ph37 Pt4	Ph39 Pt1	Ph39 Pt2	Ph39 Pt3	Ph39 Pt4	Ph44 Pt1	Ph44 Pt2	Ph44 Pt3	Ph44[a] Pt4
SiO_2	63.90	65.02	57.93	63.75	63.79	58.01	65.20	64.27	63.11
Al_2O_3	22.13	22.82	27.66	22.24	22.04	28.66	23.70	21.97	22.56
K_2O	1.24	1.52	0.46	1.38	1.19	0.35	1.23	1.17	1.23
Na_2O	8.65	9.08	6.66	8.93	9.18	6.57	8.78	8.74	8.67
CaO	3.53	3.07	8.00	2.99	3.07	9.03	3.61	3.37	3.50
MgO	0.00	0.00	0.00	0.03	0.00	0.00	0.00	0.00	0.02
TiO_2	0.00	0.06	0.06	0.03	0.00	0.03	0.10	0.04	0.02
FeO	0.00	0.16	0.26	0.04	0.04	0.08	0.12	0.00	0.00
BaO	0.02	0.15	0.29	0.14	0.00	0.14	0.07	0.03	0.11
Total	99.48	101.88	101.33	99.54	99.31	102.86	102.82	99.59	99.22
QZ	–	–	–	–	–	–	–	–	–
OR	7.17	8.49	2.67	7.93	6.71	1.94	6.99	6.80	7.13
AB	75.73	77.11	58.47	77.68	78.74	55.71	75.76	76.81	75.92
AN	17.10	14.40	38.86	14.39	14.56	42.35	17.25	16.39	16.94

[a] Ph = photo number, Pt = point number.

Table 4c. Magnetite.

Oxide	Ph1 Pt1	Ph1 Pt2	Ph1 Pt3	Ph2 Pt1	Ph2 Pt2	Ph3 Pt1	Ph3 Pt2	Ph3 Pt3	Ph3 Pt4	Ph21 Pt1	Ph21[a] Pt2
SiO_2	0.05	0.04	0.03	0.09	0.00	0.04	0.10	0.08	0.00	0.20	0.07
Al_2O_3	0.51	0.51	0.49	0.53	0.40	0.51	0.93	2.03	0.48	0.94	1.11
K_2O	–	–	–	–	–	–	–	–	–	–	–
Na_2O	–	–	–	–	–	–	–	–	–	–	–
CaO	–	–	–	–	–	–	–	–	–	–	–
FeO	75.05	75.49	76.42	75.42	73.99	77.13	89.96	89.12	76.12	85.98	87.01
MgO	0.04	0.08	0.00	0.04	0.05	0.06	0.00	0.04	0.04	0.30	0.13
MnO	0.92	0.70	0.69	0.74	0.51	0.80	0.40	0.15	0.59	3.00	2.22
TiO_2	16.10	16.94	15.66	14.57	16.20	14.16	0.47	0.24	15.85	1.81	1.64
F	–	–	–	–	–	–	–	–	–	–	–
Cl	–	–	–	–	–	–	–	–	–	–	–
Total	92.67	93.76	93.29	91.39	91.15	92.70	91.86	91.66	93.08	92.23	92.18
Ti/Fe	0.193	0.202	0.185	0.174	0.197	0.165	0.005	0.002	0.187	0.019	0.017
Mg/Mg+Fe	0.001	0.002	0.000	0.001	0.001	0.001	0.000	0.001	0.001	0.006	0.003
Ulvospinel	0.474	0.495	0.459	0.435	0.488	0.415	0.008	0.005	0.309	0.004	0.012
Magnetite	0.526	0.505	0.541	0.565	0.512	0.585	0.992	0.995	0.691	0.996	0.988

[a] Ph = photo number, Pt = point number.

Table 4d. Zircon.

Oxide	Ph24 Pt1[a]
SiO_2	31.73
Al_2O_3	0.00
K_2O	0.04
Na_2O	0.03
CaO	0.04
FeO	0.18
MgO	0.05
MnO	0.06
TiO_2	0.12
F	–
Cl	–
ZrO_2	65.79
Total	98.04

[a]Ph = photo number, Pt = point number.

Table 4b. Plagioclase.

Oxide	Ph12 Pt1	Ph12 Pt2	Ph12 Pt3	Ph12 Pt4	Ph28 Pt1	Ph28 Pt2	Ph37 Pt1	Ph37 Pt2	Ph37[a] Pt3
SiO_2	65.47	66.35	65.96	65.16	61.87	63.44	65.28	65.90	68.62
Al_2O_3	22.67	22.40	21.58	21.83	22.30	23.15	23.72	23.41	18.87
K_2O	1.09	1.47	1.23	1.25	0.68	0.67	1.26	1.28	0.83
Na_2O	8.93	9.16	9.10	8.95	8.38	8.74	8.59	8.73	7.62
CaO	2.84	2.63	2.50	2.65	3.98	3.99	3.59	3.48	2.54
MgO	0.00	0.00	0.00	0.00	0.14	0.02	0.00	0.00	0.00
TiO_2	0.00	0.04	0.00	0.00	0.00	0.08	0.00	0.08	0.03
FeO	0.20	0.16	0.24	0.04	0.48	0.32	0.23	0.12	0.06
BaO	0.00	0.00	0.04	0.02	0.00	0.00	0.00	0.08	0.00
Total	101.20	102.20	100.65	99.90	97.84	100.41	102.65	103.08	98.57
QZ	–	–	–	–	–	–	–	–	–
OR	6.39	8.35	7.17	7.34	4.06	3.89	7.27	7.35	5.69
AB	79.58	79.07	80.59	79.62	75.97	76.72	75.32	75.90	79.64
AN	14.02	12.57	12.24	13.04	19.97	19.40	17.41	16.74	14.67

Oxide	Ph37 Pt4	Ph39 Pt1	Ph39 Pt2	Ph39 Pt3	Ph39 Pt4	Ph44 Pt1	Ph44 Pt2	Ph44 Pt3	Ph44[a] Pt4
SiO_2	63.90	65.02	57.93	63.75	63.79	58.01	65.20	64.27	63.11
Al_2O_3	22.13	22.82	27.66	22.24	22.04	28.66	23.70	21.97	22.56
K_2O	1.24	1.52	0.46	1.38	1.19	0.35	1.23	1.17	1.23
Na_2O	8.65	9.08	6.66	8.93	9.18	6.57	8.78	8.74	8.67
CaO	3.53	3.07	8.00	2.99	3.07	9.03	3.61	3.37	3.50
MgO	0.00	0.00	0.00	0.03	0.00	0.00	0.00	0.00	0.02
TiO_2	0.00	0.06	0.06	0.03	0.00	0.03	0.10	0.04	0.02
FeO	0.00	0.16	0.26	0.04	0.04	0.08	0.12	0.00	0.00
BaO	0.02	0.15	0.29	0.14	0.00	0.14	0.07	0.03	0.11
Total	99.48	101.88	101.33	99.54	99.31	102.86	102.82	99.59	99.22
QZ	–	–	–	–	–	–	–	–	–
OR	7.17	8.49	2.67	7.93	6.71	1.94	6.99	6.80	7.13
AB	75.73	77.11	58.47	77.68	78.74	55.71	75.76	76.81	75.92
AN	17.10	14.40	38.86	14.39	14.56	42.35	17.25	16.39	16.94

[a] Ph = photo number, Pt = point number.

Table 4f. Matrix.

Oxide	Ph46 Pt1	Ph46 Pt2	Ph46 Pt3	Ph46 Pt4	Ph47 Pt1	Ph47[a] Pt2
SiO_2	79.57	74.30	73.64	84.36	78.18	78.84
Al_2O_3	13.30	14.42	13.73	8.82	13.03	11.91
K_2O	1.20	7.72	7.90	0.77	4.61	3.31
Na_2O	5.41	2.83	2.82	3.66	3.99	4.04
CaO	1.11	0.14	0.16	0.73	0.33	0.44
MgO	0.00	0.00	0.05	0.01	0.02	0.02
FeO	0.28	1.16	0.11	0.38	0.52	0.44
TiO_2	0.11	0.13	0.07	0.00	0.15	0.22
MnO	0.00	0.00	0.01	0.02	0.00	0.11
BaO	0.08	0.18	0.04	0.00	0.11	0.16
Total	101.07	100.89	98.53	98.77	100.82	99.49
QZ	38.76	26.23	25.37	56.95	34.25	39.95
OR	7.21	47.39	48.08	4.79	27.73	20.38
AB	49.21	26.33	26.04	34.64	36.46	37.70
AN	4.82	0.05	0.51	3.62	1.66	1.97

[a]Ph = photo number, Pt = point number.

Table 4g. Pumice.

Oxide	Ph38 Pt1	Ph43 Pt1	Ph43 Pt2	Ph45 Pt1	Ph45 Pt2	Ph45 Pt3	Ph45[a] Pt4
SiO_2	87.69	81.25	77.12	86.84	83.14	89.69	78.39
Al_2O_3	8.18	12.23	12.55	8.14	11.50	5.31	13.20
K_2O	0.44	2.72	4.94	1.88	0.55	1.43	0.68
Na_2O	3.64	4.33	3.77	2.92	4.94	1.95	6.04
CaO	0.76	0.54	0.37	0.47	1.12	0.30	1.29
MgO	0.01	0.00	0.03	0.00	0.00	0.00	0.00
FeO	0.80	0.21	0.07	0.08	0.12	0.09	0.25
TiO_2	0.09	0.09	0.05	0.05	0.08	0.07	0.01
MnO	0.00	0.00	0.00	0.00	0.00	0.03	0.02
BaO	0.06	0.00	0.12	0.10	0.04	0.25	0.00
Total	101.68	101.36	99.03	100.48	101.50	99.12	99.88
QZ	59.81	41.81	33.56	59.08	47.01	71.26	35.16
OR	2.67	16.28	29.94	11.48	3.29	8.99	4.02
AB	33.62	39.38	34.60	27.03	44.75	18.60	54.38
AN	3.90	2.53	1.90	2.41	4.95	1.14	6.44

[a]Ph = photo number, Pt = point number.

Table 5. Quantitative electron microprobe analyses of phases contained in the polished core wafer Tpt CWO_c.

Table 5a. Sanidine.

Oxide	Ph4 Pt1	Ph4 Pt2	Ph4 Pt3	Ph5 Pt4	Ph5 Pt5	Ph5 Pt6	Ph6 Pt7	Ph6 Pt8	Ph6 Pt9	Ph6 Pt10	Ph6[a] Pt11
SiO_2	64.90	66.60	65.50	66.56	66.24	64.96	64.88	65.08	65.11	65.57	65.79
Al_2O_3	19.16	17.83	17.91	18.22	18.65	18.57	19.01	19.13	19.22	20.15	19.37
K_2O	10.30	10.27	10.53	10.73	10.15	10.12	10.08	10.40	10.28	10.22	10.36
Na_2O	4.32	4.46	4.17	4.55	4.71	4.67	4.81	4.96	4.74	4.88	4.93
CaO	0.14	0.10	0.12	0.09	0.15	0.19	0.24	0.23	0.23	0.20	0.28
MgO	0.00	0.00	0.00	0.00	0.00	0.00	0.00	0.18	0.00	0.00	0.00
TiO_2	0.17	0.00	0.32	0.20	0.00	0.20	0.00	0.27	0.08	0.42	0.08
FeO	0.09	0.04	0.07	0.06	0.04	0.11	0.08	0.08	0.05	0.07	0.08
Total	99.05	99.28	98.62	100.44	99.94	98.82	99.10	100.33	99.71	101.51	100.89
OR	60.67	59.98	62.05	60.51	58.19	58.27	57.32	57.35	58.16	57.39	57.29
AB	38.65	39.54	37.37	39.04	41.08	40.82	41.54	41.60	40.77	41.65	41.43
AN	0.68	0.48	0.58	0.45	0.73	0.91	1.14	1.06	1.07	0.96	1.28

[a] Ph = photo number, Pt = point number.

Table 4e. Biotite.

Oxide	Ph4 Pt1	Ph4 Pt2	Ph4 Pt3	Ph4 Pt4	Ph4 Pt5	Ph11 Pt1	Ph11 Pt2	Ph11 Pt3	Ph11 Pt4	Ph20[a] Pt1
SiO_2	38.25	42.98	38.47	36.61	37.52	37.58	37.32	37.14	36.09	35.98
Al_2O_3	14.65	13.42	14.68	13.84	13.93	14.02	13.60	13.81	13.34	13.43
K_2O	9.42	9.00	9.66	9.12	9.40	9.06	8.95	9.07	9.08	8.75
Na_2O	0.48	0.45	0.52	0.46	0.51	0.62	0.56	0.62	0.62	0.52
CaO	0.004	0.004	0.004	0.03	0.05	0.02	0.02	0.29	0.02	0.05
FeO	19.39	18.58	19.01	18.35	17.71	22.10	21.46	18.76	19.09	22.24
MgO	10.80	10.43	11.67	10.71	11.55	10.96	10.69	10.50	10.34	10.99
MnO	0.71	0.65	0.64	0.70	0.67	1.14	1.31	1.29	1.26	1.90
TiO_2	4.80	3.87	4.51	4.38	4.59	4.27	4.44	4.25	4.72	4.10
F	0.07	0.00	0.06	0.04	0.05	0.05	0.08	0.00	0.06	0.04
Cl	0.00	0.00	0.00	0.00	0.00	0.00	0.00	0.00	0.00	0.00
Total	98.59	99.42	99.25	94.24	95.97	99.82	98.43	95.73	94.62	98.01
Ti/Fe	0.223	0.187	0.214	0.215	0.233	0.174	0.186	0.204	0.223	0.166
Mg/Mg+Fe	0.492	0.494	0.517	0.503	0.531	0.472	0.473	0.502	0.494	0.450

Oxide	Ph20 Pt2	Ph20 Pt3	Ph25 Pt1	Ph25 Pt2	Ph26 Pt1	Ph26 Pt2	Ph26 Pt3	Ph26 Pt4	Ph27 Pt1	Ph27[a] Pt2
SiO_2	35.77	36.45	34.55	34.86	37.31	39.83	38.62	37.84	36.53	36.50
Al_2O_3	13.31	13.15	15.40	13.34	14.46	15.07	14.69	14.41	14.03	14.95
K_2O	8.89	8.56	7.15	6.59	9.61	9.13	9.22	9.37	9.48	9.36
Na_2O	0.52	0.56	1.01	1.83	0.51	0.57	0.49	0.52	0.36	0.42
CaO	0.05	0.05	0.13	0.23	0.00	0.03	0.03	0.03	0.00	0.00
FeO	21.89	20.96	20.55	22.26	12.46	13.93	13.95	12.97	12.62	13.22
MgO	10.55	10.99	10.81	8.14	11.81	13.76	13.11	12.25	11.99	12.40
MnO	1.84	1.93	1.09	1.07	1.30	1.44	1.64	1.43	1.59	1.57
TiO_2	4.71	4.38	4.66	5.47	4.66	4.44	4.51	4.48	4.07	4.78
F	0.07	0.05	0.05	0.05	0.00	0.12	0.09	0.00	0.06	0.08
Cl	0.00	0.00	0.00	0.00	0.00	0.00	0.00	0.00	0.00	0.00
Total	96.92	97.08	95.39	93.84	92.12	98.33	96.35	93.30	90.75	93.28
Ti/Fe	0.200	0.188	0.204	0.221	0.337	0.287	0.291	0.311	0.290	0.326
Mg/Mg+Fe	0.452	0.463	0.486	0.397	0.630	0.640	0.628	0.630	0.631	0.628

[a]Ph = photo number, Pt = point number.

Table 5b. Biotite.

Oxide	Ph8 Pt1	Ph8 Pt2	Ph8 Pt3	Ph9 Pt4	Ph9[a] Pt5
SiO_2	36.54	37.18	35.18	36.33	36.23
Al_2O_3	13.29	13.02	12.93	13.28	13.13
K_2O	9.09	9.12	8.88	8.84	9.15
Na_2O	0.58	0.62	0.58	0.57	0.65
CaO	0.01	0.02	0.07	0.07	0.03
MgO	10.91	11.08	10.42	10.62	10.61
TiO_2	4.79	5.50	4.17	5.19	4.33
FeO	20.71	20.00	21.85	22.71	22.38
MnO	0.73	0.72	0.74	0.78	0.81
Total	96.67	97.26	94.83	98.39	97.32
Ti/Fe	0.208	0.247	0.172	0.206	0.174
Mg/Mg−Fe	0.484	0.497	0.459	0.455	0.458

[a] Ph = photo number, Pt = point number.

Table 5c. Magnetite.

Oxide	Ph10 Pt1	Ph10 Pt2	Ph10[a] Pt3
SiO_2	0.08	0.04	0.07
Al_2O_3	1.31	1.32	1.36
K_2O	0.00	0.00	0.00
Na_2O	0.00	0.00	0.00
CaO	0.00	0.00	0.00
MgO	0.10	0.09	0.11
TiO_2	9.90	10.28	10.05
FeO	83.13	83.95	84.89
MnO	1.77	1.74	1.83
Total	96.29	97.43	98.30
Ti/Fe	0.107	0.110	0.106
Mg/Mg−Fe	0.002	0.002	0.002

[a] Ph = photo number, Pt = point number.

Table 5d. Plagioclase.

Oxide	Ph1 Pt1	Ph1 Pt2	Ph1 Pt3	Ph2 Pt4	Ph2 Pt5	Ph2 Pt6	Ph2 Pt7	Ph2 Pt8	Ph2 Pt9	Ph3 Pt10	Ph3 Pt11	Ph3[a] Pt12
SiO_2	65.00	64.16	64.54	56.98	57.39	57.29	64.13	64.90	64.65	64.73	64.82	64.49
Al_2O_3	22.44	22.58	22.42	26.90	26.74	26.39	22.20	22.44	22.22	22.26	22.02	22.06
K_2O	1.24	1.04	1.14	0.36	0.37	0.42	1.22	1.27	1.34	0.99	1.29	1.26
Na_2O	8.96	8.94	9.02	6.44	6.57	6.46	8.87	9.51	9.07	9.27	9.11	8.99
CaO	3.57	3.91	3.87	8.68	8.81	8.01	8.87	3.43	3.37	3.48	3.57	3.60
MgO	0.00	0.00	0.00	0.00	0.00	0.00	0.00	0.00	0.00	0.00	0.00	0.00
TiO_2	0.05	0.00	0.03	0.92	0.06	0.02	0.00	0.00	0.05	0.00	0.02	0.03
FeO	0.13	0.31	0.15	0.11	0.11	0.13	0.13	0.13	0.17	0.10	0.15	0.15
Total	101.39	100.94	101.17	100.38	100.07	98.70	99.85	101.69	100.86	100.83	100.98	100.57
OR	6.92	5.83	6.32	2.04	2.11	2.47	6.98	6.85	7.46	5.51	7.09	7.04
AB	76.28	75.86	75.75	56.14	56.22	57.86	77.13	77.68	76.80	78.24	76.37	76.13
AN	18.80	18.32	17.94	41.82	41.67	39.67	15.90	15.47	15.74	16.25	16.54	16.83

[a] Ph = photo number, Pt = point number.

Figure 29 shows the variation in potassium (orthoclase molecular end member) in the alkali feldspar; Fig. 30 shows the variation in calcium (anorthite molecular end member) in plagioclase; while Fig. 31 shows the variation in the magnesium to iron ratio (Mg/Mg + Fe) in biotite. Note that these plots contain data from both the polished thin section and the polished core wafers.

The alkali feldspars analyzed from Tpt-FR had an average calculated orthoclase end member composition of OR 0.57, although the distribution is distinctly bimodal. Values ranged from a low of OR 0.46 to a high of OR 0.64; samples included phenocrysts and the products of coarse granophyric devitrification and vapor-phase deposition.

Actually, three distinct groups of compositions may be recognized in the data: phenocrysts from the crystal-rich xenolithic fragment; phenocrysts dispersed through the matrix of the rock; and coarse, granophyric devitrification products. The phenocryst-rich xenolith in the thin section (described on page 8) contained phenocrysts of alkali feldspar that are less potassic than the bulk of the alkali feldspars in Tpt-FR. This pumice fragment contains phenocrysts of alkali feldspar that range from OR 0.46 to OR 0.52, with a dominant value of OR 0.51. Although the ranges overlap considerably, compositions greater than OR 0.60 are always indicative of alkali feldspars that are small, vapor-phase altered, and coarsely granophyric. Phenocrysts of alkali feldspar are always less than this value, and the dominant value for the phenocrysts is closer to OR 0.57. Note that these alkali feldspars are quite distinct compositionally from those observed in the Bullfrog Member Tuff (Knauss, 1983); this is clearly a case where phenocryst composition could be used to identify samples of unknown or questionable origin. This difference in composition between the two units may also be seen in Warren's data (Bish et al., 1981) on samples from hole USW G-1.

The plagioclase feldspars analyzed, which were all phenocrysts, ranged in calculated anorthite end-member composition from AN 0.12 to AN 0.45, with the dominant value being AN 0.17. The distribution was bimodal, and the more calcic group had a dominant composition of AN 0.40. Lipman et al. (1966) suggested these more calcic plagioclases may in fact be xenocrysts.

The biotite phenocrysts analyzed were found to have a Mg/Mg + Fe ratio that ranged from 0.33 to 0.64, and the distribution was trimodal. Typical biotite dispersed throughout the bulk of Tpt-FR had a dominant Mg/Mg + Fe ratio of 0.47, and ranged from 0.44 to 0.53. Biotite from the

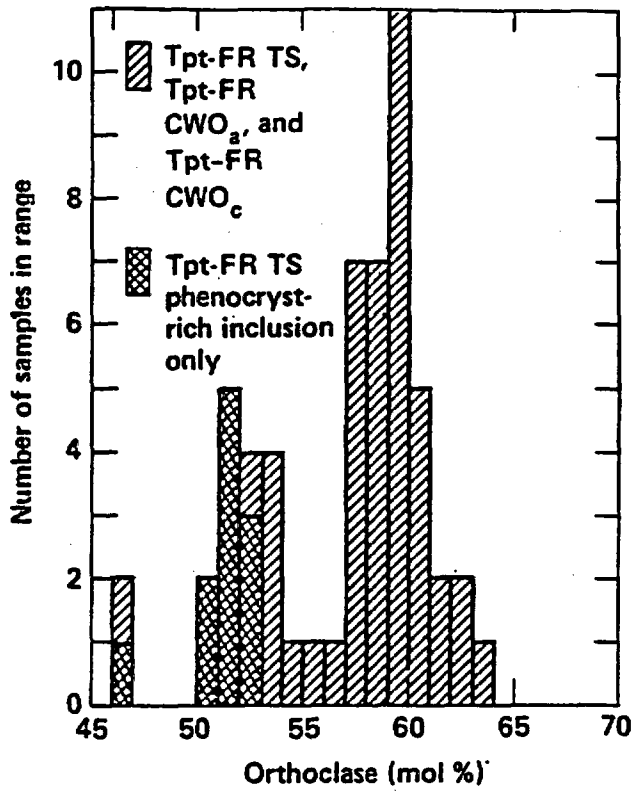

Figure 29. Ordinary histogram of calculated orthoclase in alkali feldspar phenocrysts.

phenocryst-rich xenolithic fragment was much more iron-rich, averaging Mg/Mg + Fe 0.35. The third group of analyses are represented by two small biotite fragments found in the crystal-poor matrix of one polished core wafer; these fragments were distinctly magnesium-rich with Mg/Mg + Fe values of 0.63. It should be noted that much of the biotite in Tpt-Fr is badly oxidized and altered to hematite; such areas were avoided when making analyses.

The analyses presented in this report for Tpt-FR agree very well with previously published results from the rhyolitic portions of the densely welded, devitrified Tpt both in outcrop and from drill core. Lipman et al. (1966) used indirect methods (petrographic and XRD) to estimate phenocryst compositions in outcrop samples. They found alkali feldspar to range from OR 0.47 to OR 0.60, with no differences between the rhyolitic and quartz latitic portions of the unit. These authors also found plagioclase to average AN 0.20 in the rhyolite and AN 0.25 to 0.30 in the quartz latite. Heiken and Bevier (1979) noted that in J-13 the rhyolitic densely welded Tpt contained plagioclase that ranged from AN 0.20 to 0.24. Their

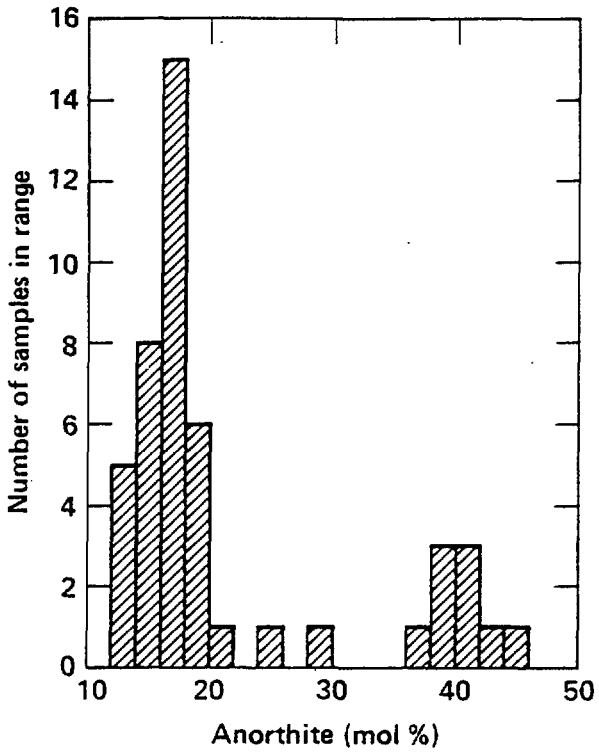

Figure 30. Ordinary histogram of calculated anorthite in plagioclase phenocrysts.

analyses of vapor-phase alkali feldspar closely resemble analyses of similar phases presented in this report. Bish et al. (1981) present analyses from the proposed repository depth in USW G-1 that show a median alkali feldspar composition of OR 0.57, a dominant plagioclase composition of AN 0.16 (range: AN 0.14 to AN 0.40), and a median biotite Mg/Mg + Fe ratio of 0.44. Carroll et al. (1981) sampled higher in the same core (i.e., USW G-1) within the densely welded tuff between the two lithophysal zones in the Tpt unit and found alkali feldspar with a mean composition of OR 0.54 (range: OR 0.47 to OR 0.58) and plagioclase feldspar with a dominant AN 0.17 (range: AN 0.15 to AN 0.33). These data from USW G-1 show that phenocrysts do not vary in composition between the densely welded tuff below the lowermost lithophysal zone and the vitrophyre and the densely welded tuff between the two lithophysal zones. In hole USW G-2 Caporuscio et al. (1982) found—for samples taken from the densely welded, rhyolitic tuff below the quartz latite and above the vitrophyre—the alkali feldspar ranged from OR 0.39 to OR 0.65 with an average of OR 0.53, the plagioclase ranged from AN 0.10 to AN 0.40 with a dominant value of AN 0.18, and the biotite analyses resembled those presented in this

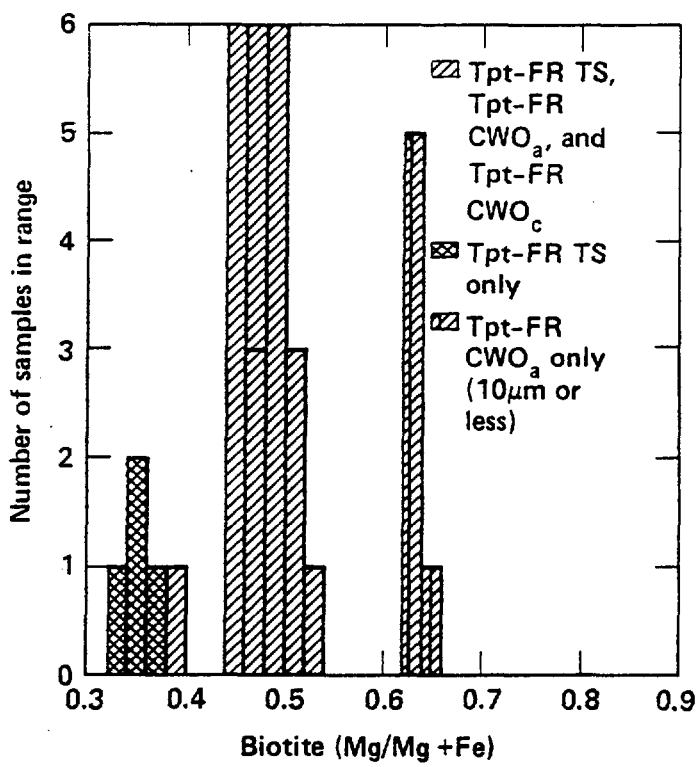

Figure 31. Ordinary histogram of measured Mg/Mg+Fe in biotite.

report. These authors found the range in biotite Mg/Mg+Fe ratio to be 0.31 to 0.82, but the distribution was controlled by two groups: one centered at 0.42 and the other centered at 0.73.

Unfortunately, the data reviewed from the published analyses to date do not suggest any way that the compositional variations in either the vitric components or the phenocrysts present in the densely welded Tpt may be used to distinguish whether the Tpt-FR position is equivalent to a location above or below the lowermost lithophysal zone. The Tpt-FR analyses presented in this report agree well with those previously published from both of the densely welded intervals in question. This fact suggests that for the purposes of Waste Package experiments with outcrop samples, it may be immaterial whether Tpt-FR is stratigraphically equivalent to the densely welded, devitrified Tpt between the lowermost lithophysal zone and the vitrophyre or equivalent to the similar Tpt between the two lithophysal zones. The data presented in this report do, however, show that the phenocryst-rich xenolith does contain alkali feldspar and biotite that are compositionally distinct from those encountered in the bulk of the Tpt-FR samples.

Summary

The purpose of this characterization of Tpt-FR is twofold: to provide data about the mineralogy and chemistry of the tuff used in experiments supporting waste package design and to verify that outcrop material is an acceptable substitute for drill core material at depth beneath Yucca Mountain within the proposed repository interval. Although it is not required for establishing the acceptability of the outcrop samples for use in the experiments, circumstantial evidence was collected to locate the relative stratigraphic position of the Tpt-FR outcrop.

The basic data provided here include the following:

- Simple petrographic description of phenocrysts and original vitric components and textures.
- Relative distribution of the dominant mineral phases.
- XRD phase identification and semiquantitative estimate of mineral phase proportions.
- SEM phase identification and vitric textures.
- Nature and distribution of fractures and fillings.
- Gas adsorption BET surface-area analyses.
- NAA chemical analyses of whole rock.
- EMP quantitative chemical analyses of phases.

These data are needed to form the baseline against which the results of component-interaction tests will be measured.

Field relationships at the Tpt-FR outcrop and at the southern end of Fran Ridge—when combined with evidence provided by petrography, XRD, and phenocryst chemistry from EMP analyses—strongly suggest that the Tpt-FR outcrop is stratigraphically equivalent to a position in the column between the two lithophysal zones in the rhyolitic, densely welded portion of the compound cooling unit.

The field evidence includes:

- The base of the lithophysal zone above UE-25h#1 was traced around the south end of Fran Ridge to the Tpt-FR outcrop.
- Hand samples from the Tpt section at both Busted Butte and above UE-25h#1 were compared with hand samples from the Tpt-FR outcrop.

The petrographic evidence includes:

- The lack of significant tridymite, except for small amounts of tridymite that is retrograded to quartz and typically results from vapor-phase deposition in cavities.

The XRD evidence includes:

- The lack of tridymite.
- The abundance of both cristobalite and quartz.

The evidence from quantitative EMP analyses of individual mineral phases includes:

- Comparison with previously published data from both outcrop and drillcore.

The evidence for relative stratigraphic position presented above places the Tpt-FR outcrop in the column in a position equivalent to that of the breakout horizon for the exploratory shaft. This location was selected in part for its mineralogic, geochemical, and structural similarity to the proposed repository unit within the exploratory block beneath Yucca Mountain.

More importantly, mineralogical and geochemical analyses to date demonstrate no real differences between the rhyolitic, densely welded

tuff above and below the lowermost lithophysal zone (Bish, 1984; Crowe, 1984; Vaniman, 1984). The mineralogical and geochemical analyses reported here demonstrate that the Tpt-FR outcrop is quite similar to tuff from drillcore from either interval. Thus, the outcrop samples used in Waste Package experiments should be an acceptable substitute. The outcrop samples taken from Tpt-FR do, however, contain trace amounts of evaporite minerals (carbonates, borates, sulfates, nitrates, etc.) from precipitation from meteoric water (Knauss et al., 1983). Where it is essential to remove these from the rock before experimental work, a simple leaching procedure will effectively remove these salts without affecting the tuff itself. The primary use for the outcrop samples from Tpt-FR is for experiments where either large quantities or large-diameter samples are required. For the package environment subtask, the hydrothermal rock/water interaction experiments conducted in rocking autoclaves, which will be modeled by the geochemical modeling code EQ3/6, use drillcore samples from the proposed repository depth beneath Yucca Mountain.

Acknowledgments

The acquisition and characterization of the outcrop samples described in this report required the help of many individuals. Bruce Crowe suggested the outcrop location, and he and Kirk Keller and Carl Boro helped in sample collection. Bill Beiriger helped in sample preparation and assisted in the SEM examination and the EMP analysis of the polished core wafers. Chuck Slettevold made the gas adsorption BET measurements. Gayle Pawloski made the XRD analyses. Barbara Bryan and Sue Frumenti typed the tables of microprobe analyses. For the NAA analysis, Jan Brown prepared the samples and Bob Heft performed the analysis. Virginia Oversby provided constructive criticism and many valuable suggestions. Rick Ryerson helped in many ways in the operation of the JEOL 733 electron microprobe. Dave Bish, Bruce Crowe, and Dave Vaniman provided information on the petrology of the repository horizon, the quantification of XRD analyses, and structural relationships at the Yucca Mountain site.

References

Bence, A. E., and A. L. Albee (1968), "Empirical correction factors for the electron microanalysis of silicates and oxides," *J. Geol.* 76, 382–403.

Bish, D. L., F. A. Caporuscio, J. F. Copp, B. M. Crowe, J. D. Purson, J. R. Smyth, and R. G. Warren (1981), *Preliminary Stratigraphic and Petrologic Characterization of Core Samples from USW-G1, Yucca Mountain, Nevada,* Los Alamos National Laboratory, Los Alamos, NM, LA-8840-MS.

Bish, D. L., A. E. Ogard, D. T. Vaniman, and L. V. Benson (1984), *Mineralogy-Petrology and Groundwater Geochemistry of Yucca Mountain Tuffs,* Los Alamos National Laboratory, Los Alamos, NM, LAUR-84-332.

Bish, D.L. (1984), Los Alamos National Laboratory, Los Alamos, NM, personal communication.

Broxton, D., D. Vaniman, F. Caporuscio, B. Arney, and G. Heiken (1982), *Detailed Petrographic Descriptions and Microprobe Data for Drill Holes USW-G2 and UE-25b#1h, Yucca Mountain, Nevada,* Los Alamos National Laboratory, Los Alamos, NM, LA-9324-MS.

Caporuscio, F., D. Vaniman, D. Bish, D. Broxton, B. Arney, G. Heiken, F. Byers, R. Gooley, and E. Semarge (1982), *Petrologic Studies of Drill Cores USW-G2 and UE-25b#1h, Yucca Mountain, Nevada,* Los Alamos National Laboratory, Los Alamos, NM, LA-9255-MS.

Carroll, P. I., F. A. Caporuscio, and D. L. Bish (1981), *Further Description of the Petrology of the Topopah Spring Member of the Paintbrush Tuff in Drill Holes UE-25a#1 and USW-G1 and the Lithic-Rich Tuff in USW-G1, Yucca Mountain, Nevada,* Los Alamos National Laboratory, Los Alamos, NM, LA-9000-MS.

Crowe, B. M. (1984), Los Alamos National Laboratory, Los Alamos, NM, personal communication.

Gunnink, R., and J. B. Niday (1972), *Computerized Quantitative Analysis by Gamma-Ray Spectrometry, Description of the GAMANAL Program,* Lawrence Livermore National Laboratory, Livermore, CA, UCRL-51061, vol. 1.

Heft, R. E., and W. H. Martin (1977), *NADAC and MERGE: Computer Codes for Processing Neutron Activation Analysis Data,* Lawrence Livermore National Laboratory, Livermore, CA, UCRL-52249.

Heiken, G. H., and M. L. Bevier (1979), *Petrology of Tuff Units from the J-13 Drill Site, Jackass Flats, Nevada,* Los Alamos National Laboratory, Los Alamos, NM, LA-7563-MS.

Knauss, K. G., V. M. Oversby, and T. J. Wolery (1983), *Post-Emplacement Environment of Waste Packages,* Lawrence Livermore National Laboratory, Livermore, CA, UCRL-89425.

Knauss, K. G. (1983), *Petrologic and Geochemical Characterization of the Bullfrog Member of the Crater Flat Tuff: Outcrop Samples Used in Waste Package Experiments,* Lawrence Livermore National Laboratory, Livermore, CA, UCRL-53470.

Knauss, K. G. (1984), *Hydrothermal Interaction Studies of Bullfrog Member Tuff Core Wafers in J-13 Water at 150°C—Quantitative Analyses of Aqueous and Solid Phases,* Lawrence Livermore National Laboratory, Livermore, CA, UCRL-53521.

Knauss, K. G. (1984), *Geochemical Variability Within the Near-Field Environment of the Potential Repository in the Topopah Spring Member,* Lawrence Livermore National Laboratory, Livermore, CA, UCRL report in preparation.

Lipman, P. W., and E. J. McKay (1965), *Geologic Map of the Topopah Spring SW Quadrangle, Nye County, Nevada,* US Geological Survey Map GQ-439.

Lipman, P. W., R. L. Christiansen, and J. T. O'Connor (1966), *A Compositionally Zoned Ash Flow Sheet in Southern Nevada,* US Geological Survey Professional Paper 524-F.

Oversby, V. M., and K. G. Knauss (1983), *Reaction of Bullfrog Tuff with J-13 Water at 90°C and 150°C,* Lawrence Livermore National Laboratory, Livermore, CA, UCRL-53442.

Scott, B., and M. Castellanos (1983), *Preliminary Report on the Geologic Character of Drill Holes USW-GU3 and USW-G3,* Memorandum Report to Gary Dixon, US Geological Survey.

Spengler, R. W., F. M. Byers, Jr., and J. B. Warner (1981), *Stratigraphy and Structure of Volcanic Rocks in Drill Hole USW-G1, Yucca Mountain, Nye County, Nevada,* US Geological Survey Open File Report 81-1349.

Sykes, M. L., G. H. Heiken, and J. R. Smyth (1979), *Mineralogy and Petrology of Tuff Units from the UE-25a#1 Drill Site, Yucca Mountain, Nevada,* Los Alamos National Laboratory, Los Alamos, NM, LA-8139-MS.

Tyler, L. D. (1982), Memorandum from L. D. Tyler of SNL to Don Veith of WMPO, NNWSI, July 9, 1982.

Vaniman, D. T. (1984), Los Alamos National Laboratory, Los Alamos, NM, personal communication.

Technical Information Department · Lawrence Livermore National Laboratory
University of California · Livermore, California 94550

Return Postage Guaranteed

United States Department of Energy
Office of Scientific and Technical Information
Post Office Box 62
Oak Ridge, Tennessee 37831

OFFICIAL BUSINESS
PENALTY FOR PRIVATE USE, $300

POSTAGE AND FEES PAID
DEPARTMENT OF ENERGY
DOE-350

U S MAIL

12359 FS- 1
SCIENCE APPLICATION INC
ATTN LIBRARY
2769 S HIGHLAND DR
LAS VEGAS, NV 89109